

Guest Lecture

# Machine Learning in Healthcare

Narges Razavian

Assistant Professor

Departments of Radiology & Population Health NYUMC

[narges.razavian@nyumc.org](mailto:narges.razavian@nyumc.org)

*Machine Learning*  
*November 1st, 2018*

# This Lecture

Overview of healthcare & landscape of healthcare data

Some snapshots of research on machine learning in healthcare

*Early Disease Prediction using EHR time series*

*Medical Imaging:*

*Radiology (X-Rays, Mammograms, MRI, Ultrasound)*

*Pathology (Histopathology)*

*Microscopy*

Genomics and sequences and text

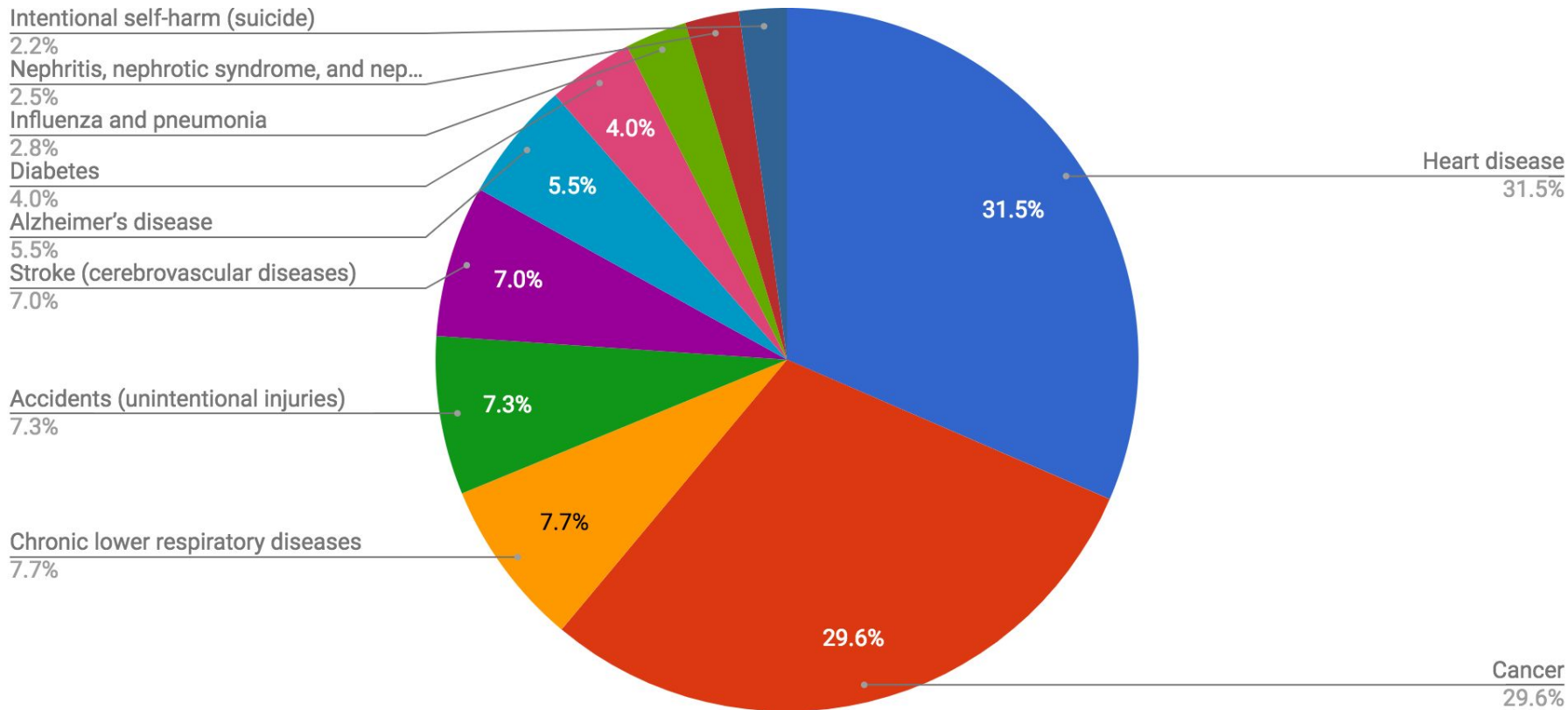
Thoughts on research trends in short and long term in this field.

# Healthcare in Numbers

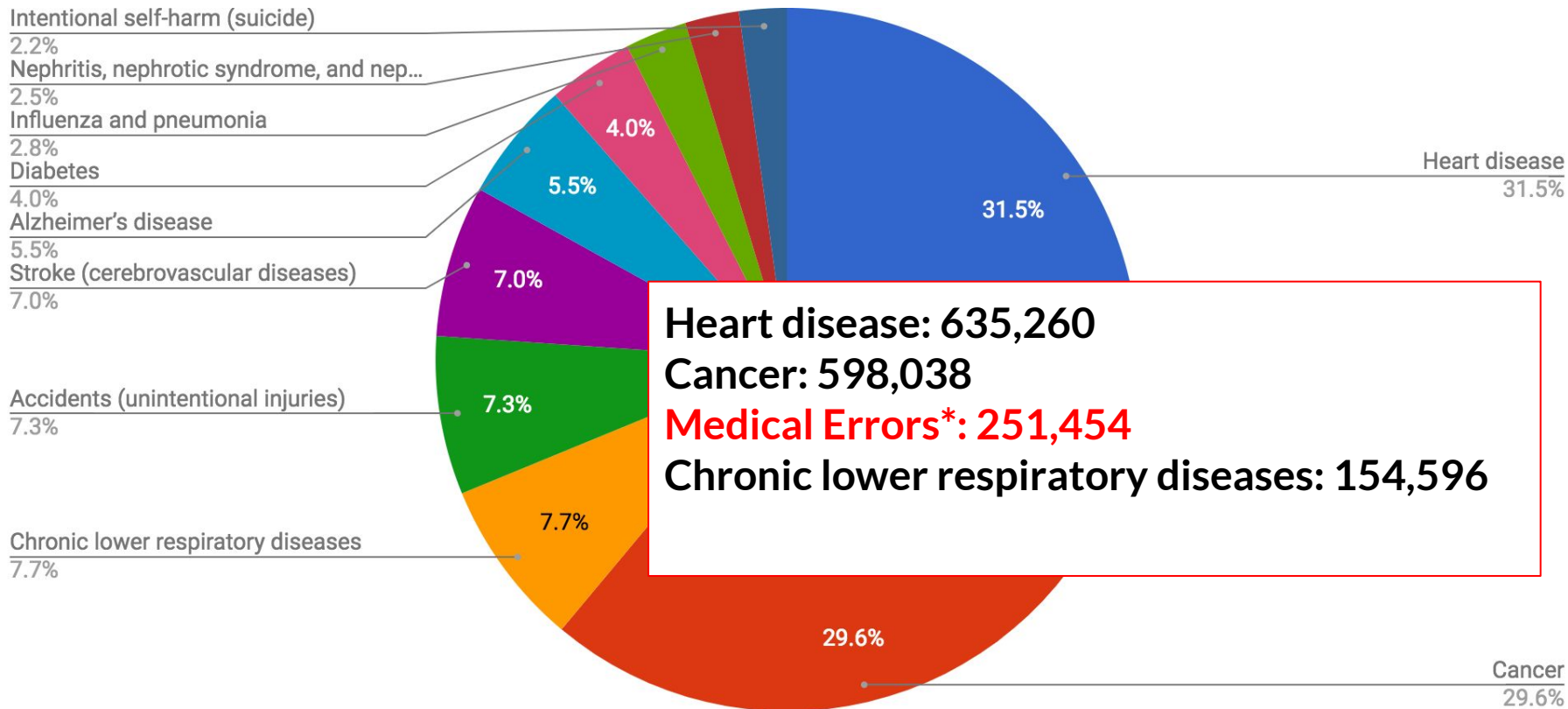
What are the top killer diseases?

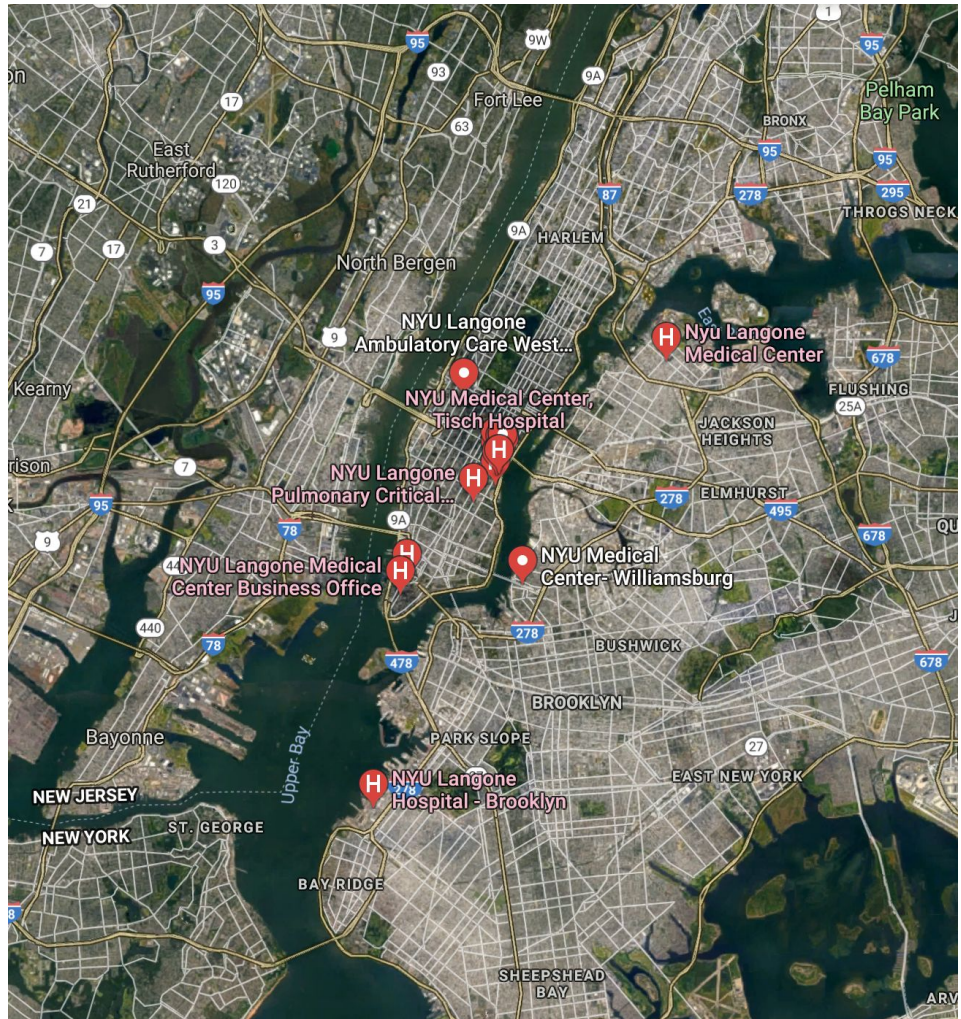
What are the diseases people go to doctors for?

# “Immature” Causes of Death in 2016, USA

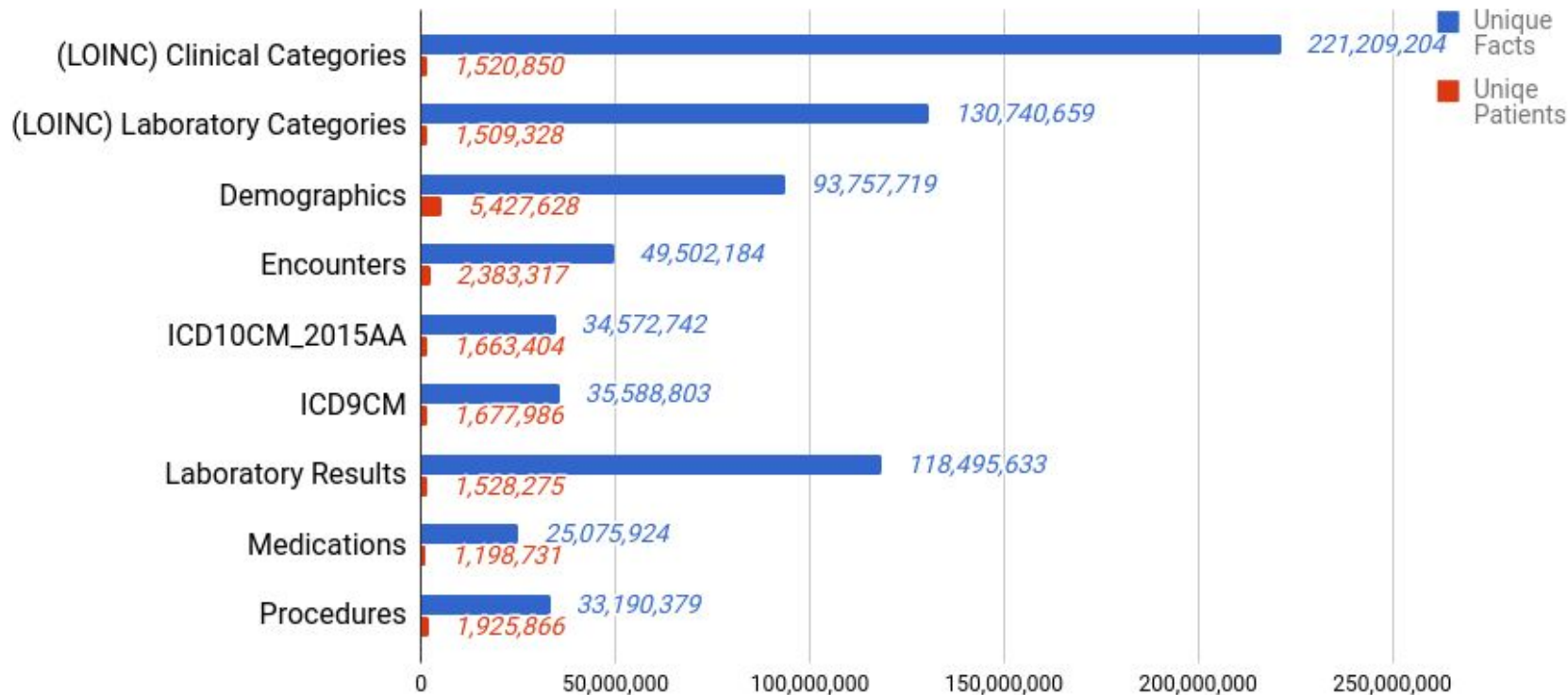


# “Immature” Causes of Death in 2016, USA

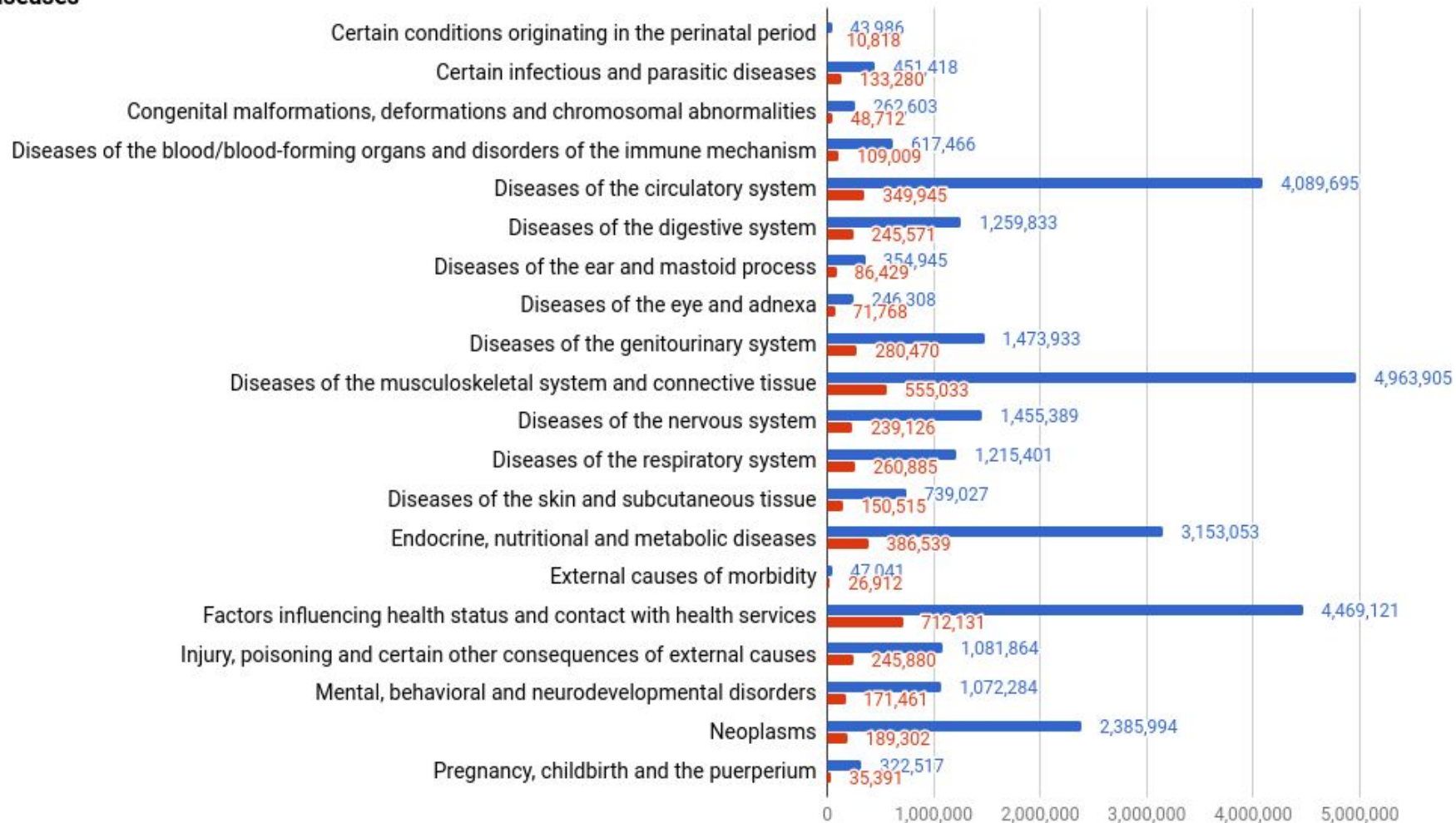




# NYU Medical School - de-identified database i2b2 (2 years ago)

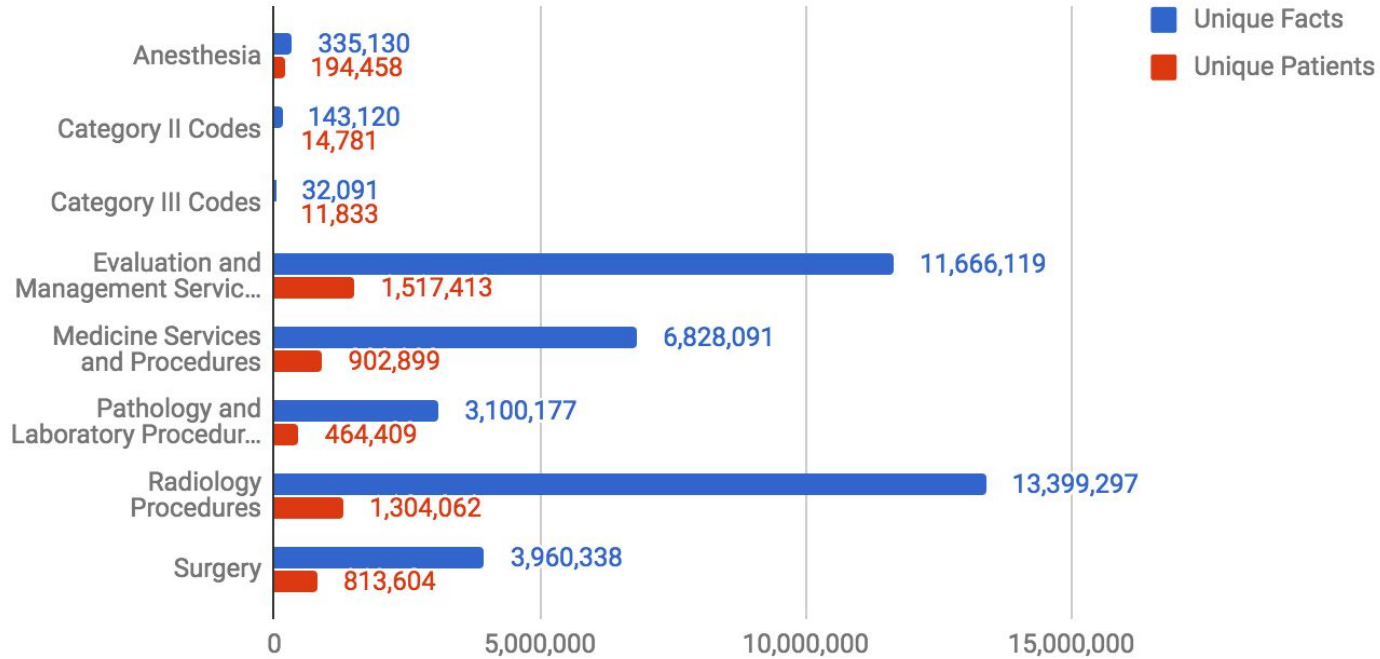


## Diseases





# Procedures

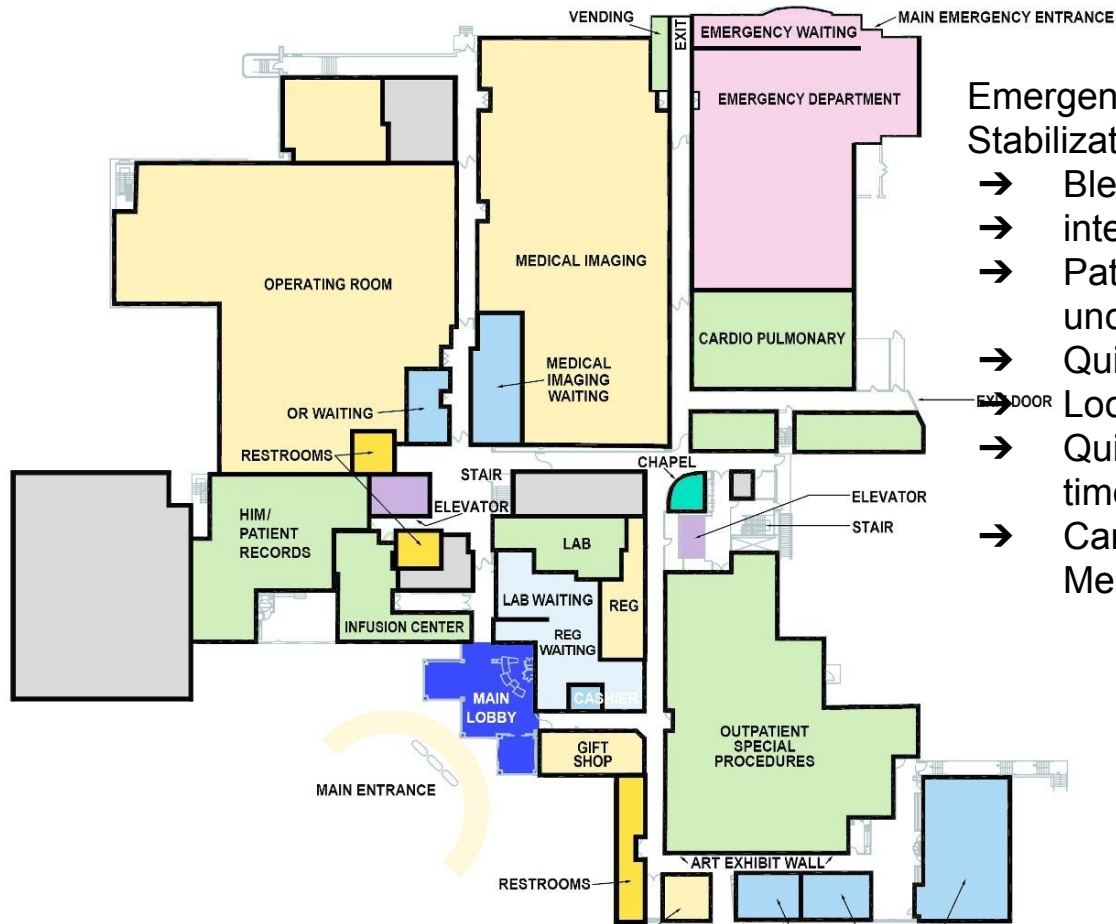


# Healthcare in Action

What happens Where and When?

What's the constraints of each location?

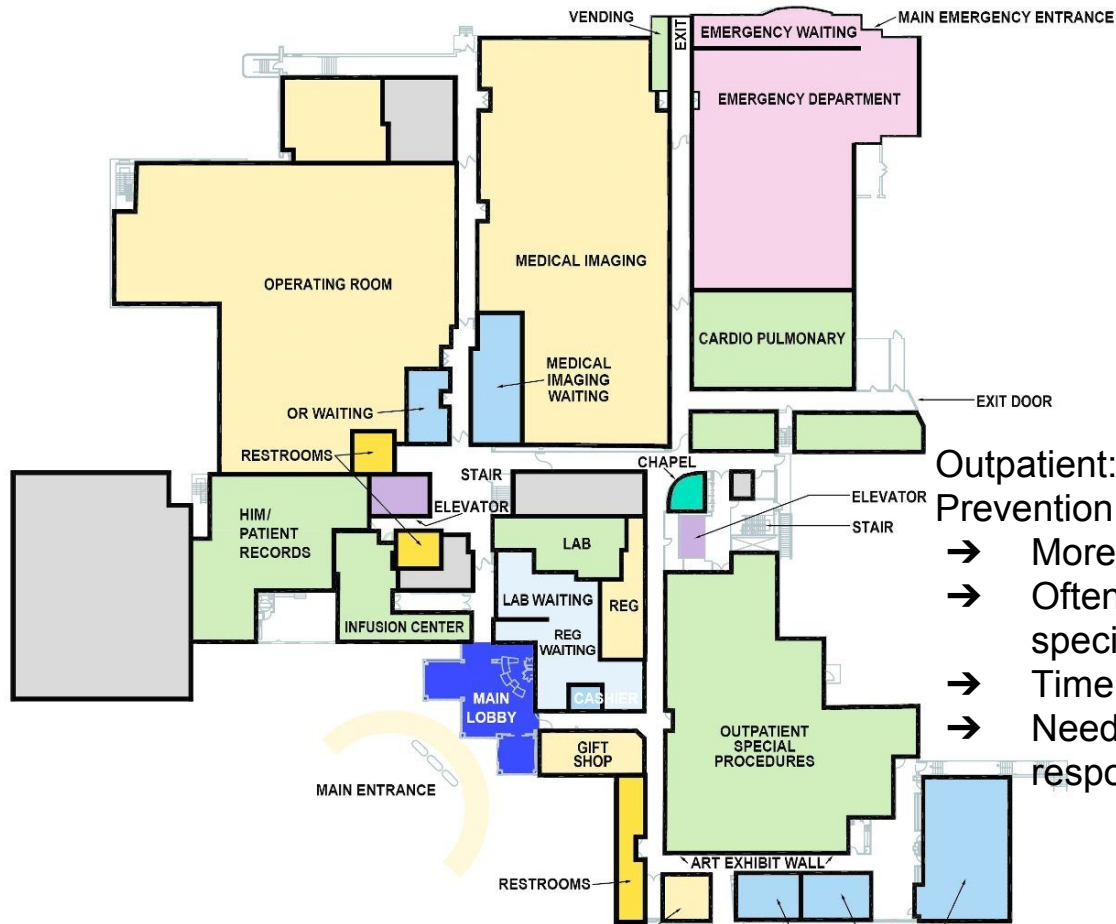
# Overview of Healthcare in Action



Emergency Dept: Triage & Stabilization

- Bleeding/pain/etc
- internal/external problems
- Patient awake or unconscious
- Quick diagnosis needed
- Localization of main cause
- Quick action to give patient time
- Can be: Fast, Noisy, Loud, Mechanical

# Overview of Healthcare in Action



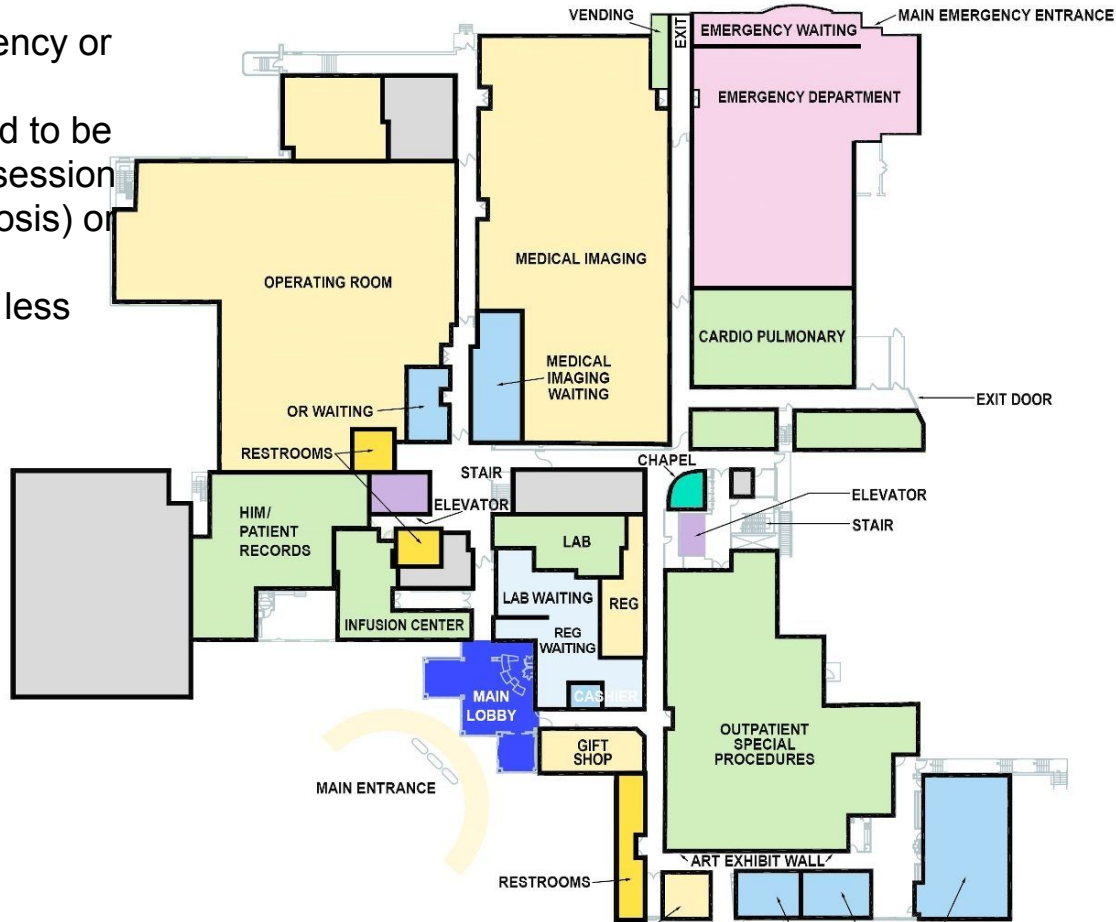
Outpatient: Diagnosis, Curing and Prevention

- More time to diagnose
- Often symptoms aren't specific/strong enough
- Time to do (diagnostic) tests
- Need to track medication response or Prevent s.th.

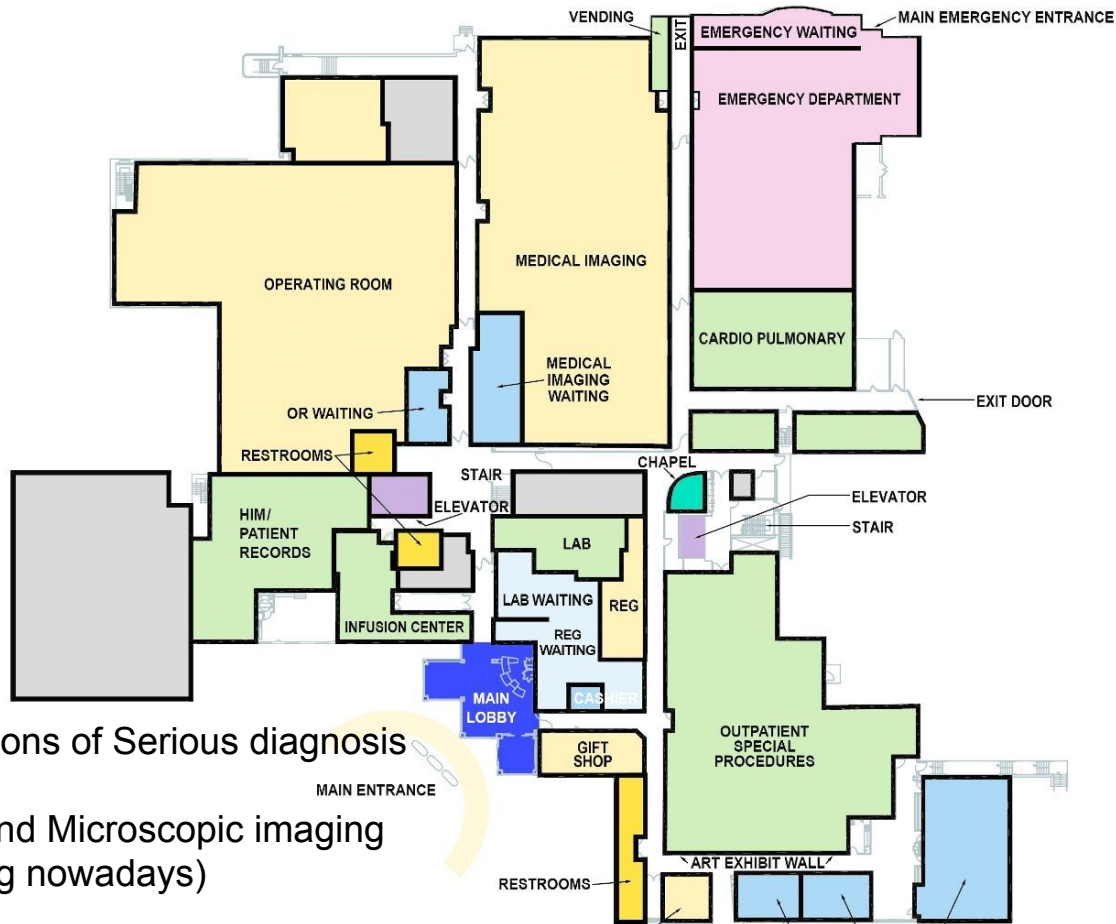
# Overview of Healthcare in Action

Surgery: Either Emergency or Elected

- Invasive and need to be complete in one session
- For biopsy(diagnosis) or treatment
- *Robotic Surgery*: less invasive.



# Overview of Healthcare in Action

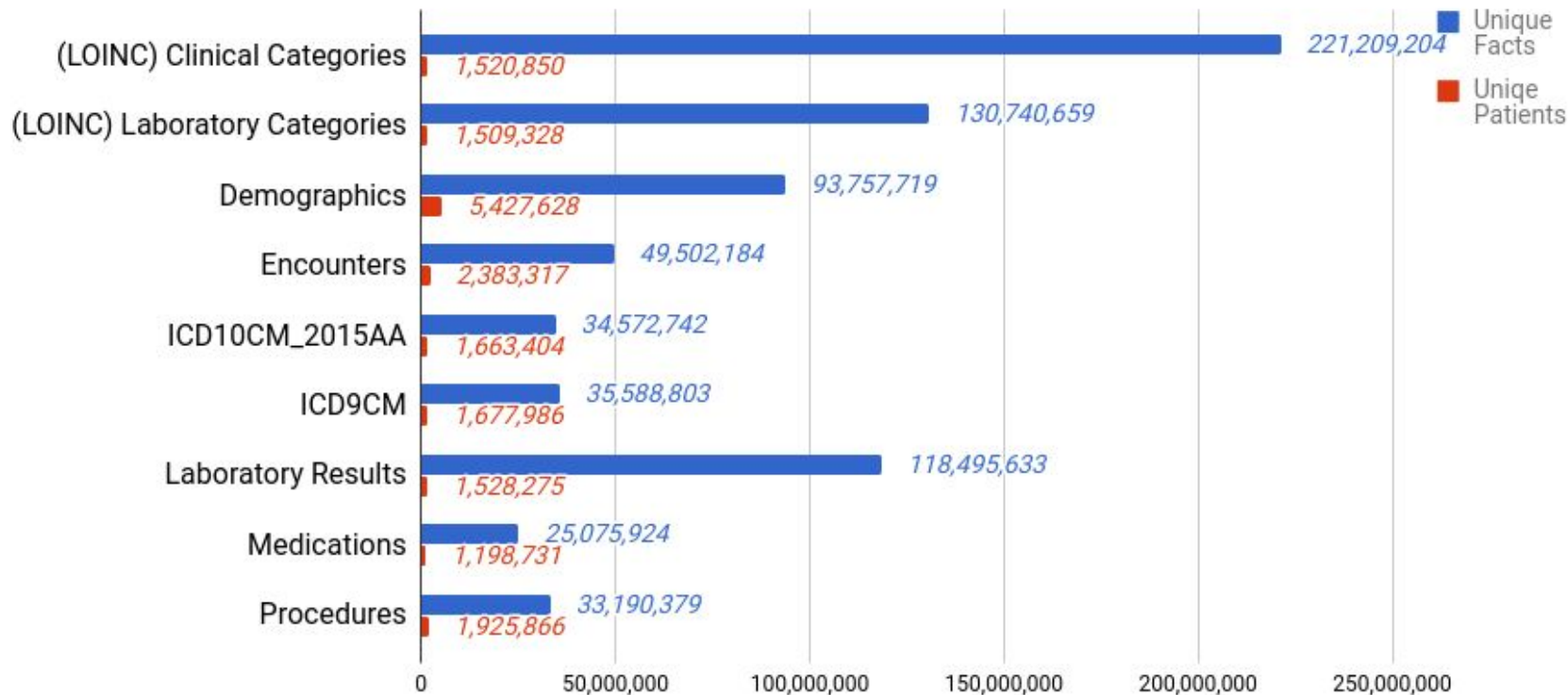


Pathology: Confirmations of Serious diagnosis

- Most cancers,
- Tissues, cells and Microscopic imaging
- (Genetic reading nowadays)

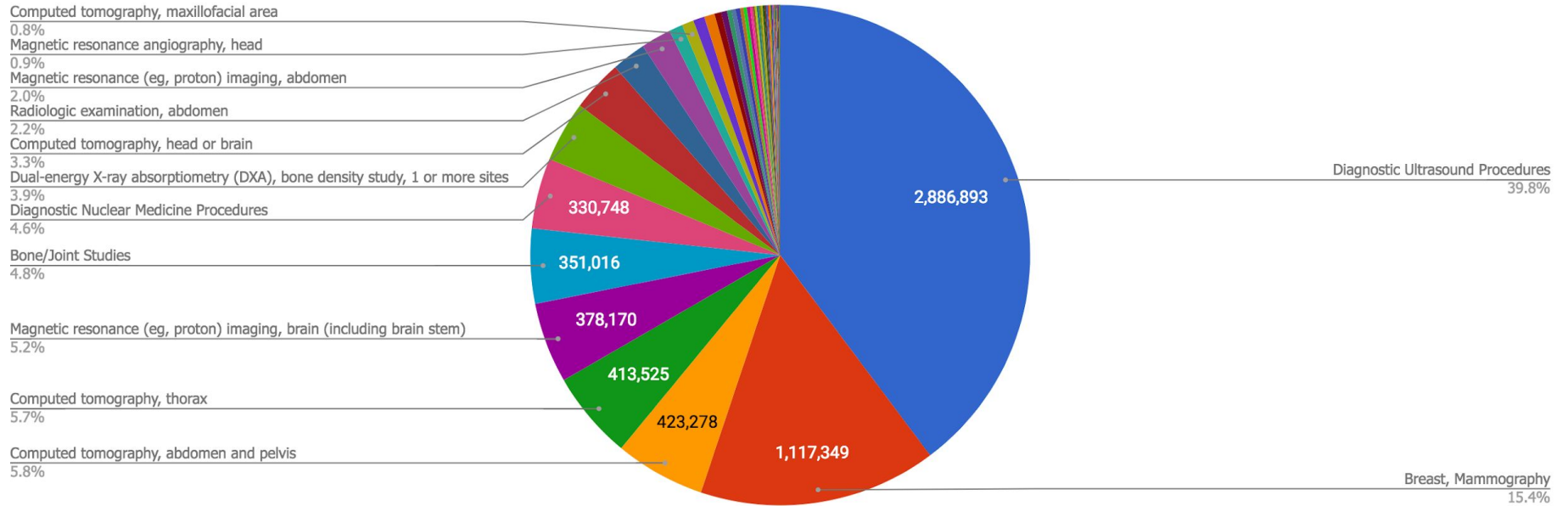
# Diverse Data Modalities

# Diverse Modalities: Text and Structured data Time Series (NYU Data)





# Diverse Modalities: Images (NYU data)



# Diverse Modalities: Genomics (Public GDC data)

Harmonized Cancer Datasets

## Genomic Data Commons Data Portal

Get Started by Exploring:



Q e.g. BRAF, Breast, TCGA-BLCA, TCGA-A5-A0G2

### Data Portal Summary [Data Release 10.1 - February 15, 2018](#)

PROJECTS



40

PRIMARY SITES



61

CASES



32,555

FILES



310,859

GENES

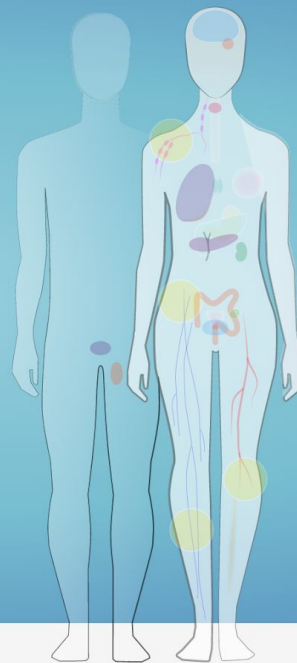


22,147

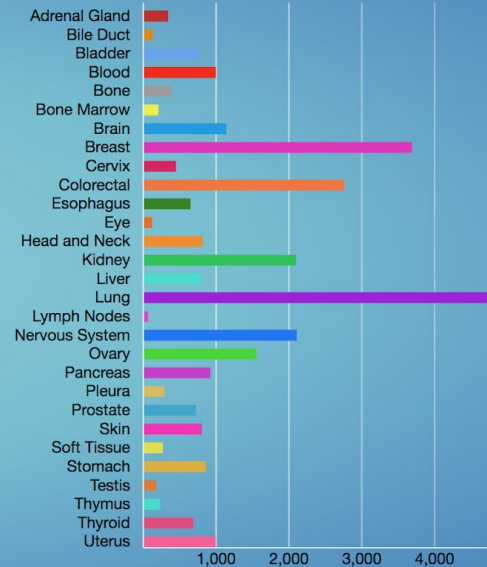
MUTATIONS



3,142,246



Cases by Major Primary Site



What else?

# Questions that Could Use More ML in Healthcare

Early detection, Detection, and Prevention

Automated/Augmented Diagnosis/screening & Lowering medical errors

Finding new bio-makers, less invasive, more specific & sensitive, scalable

Better clinical trial recruitment - faster drug design

Tracking Treatment Response and Disease Progression

Finding, measuring, and visualizing biomarker & changes over time

Low resource settings & where time is limited i.e. ED department

Prioritization of patients

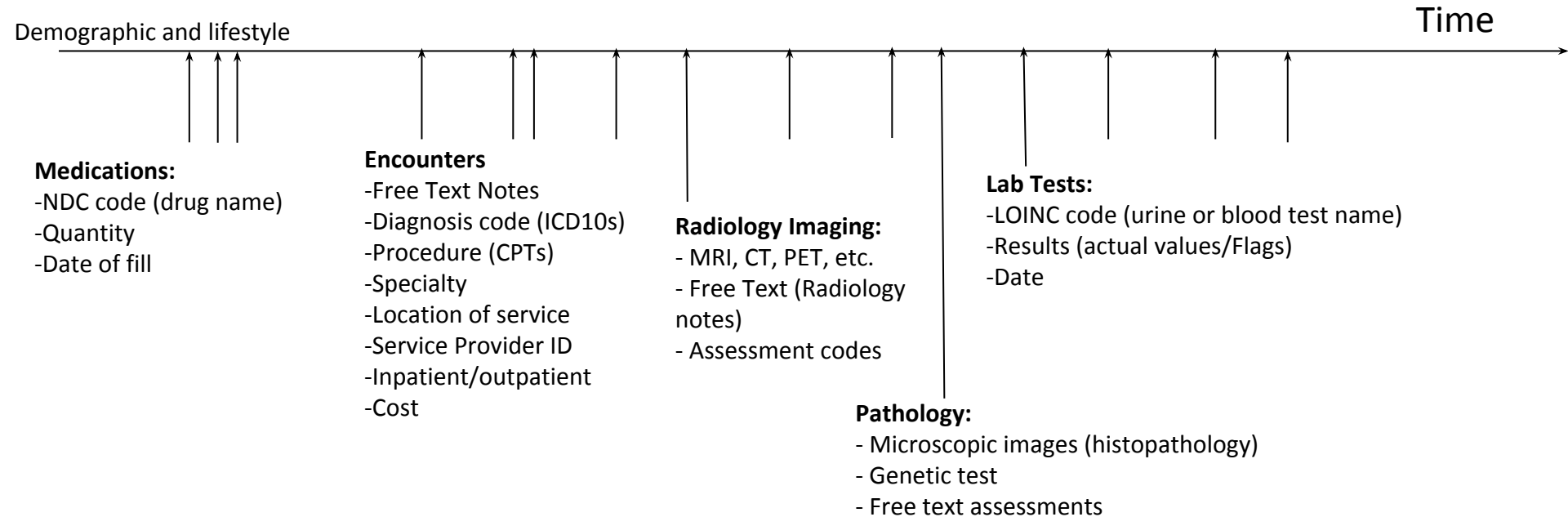
Lowering missed diagnosis - augmented diagnosis, automations, etc

What else?

Some snapshots of research on machine  
learning in healthcare

# Early Disease Prediction using EHR time series

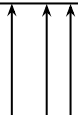
# Electronic Health Records



# Electronic Health Records

Time

Demographic and lifestyle



## Medications:

- NDC code (drug name)
- Quantity
- Date of fill

## Encounters

- Free Text Notes
- Diagnosis code (ICD10s)
- Procedure (CPTs)
- Specialty
- Location of service
- Service Provider ID
- Inpatient/outpatient
- Cost

## Radiology Imaging:

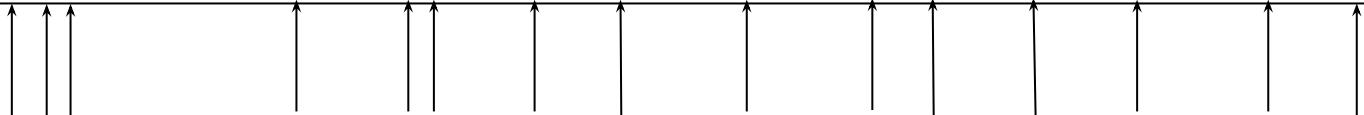
- MRI, CT, PET, etc.
- Free Text (Radiology notes)
- Assessment codes

## Pathology:

- Microscopic images (histopathology)
- Genetic test
- Free text assessments

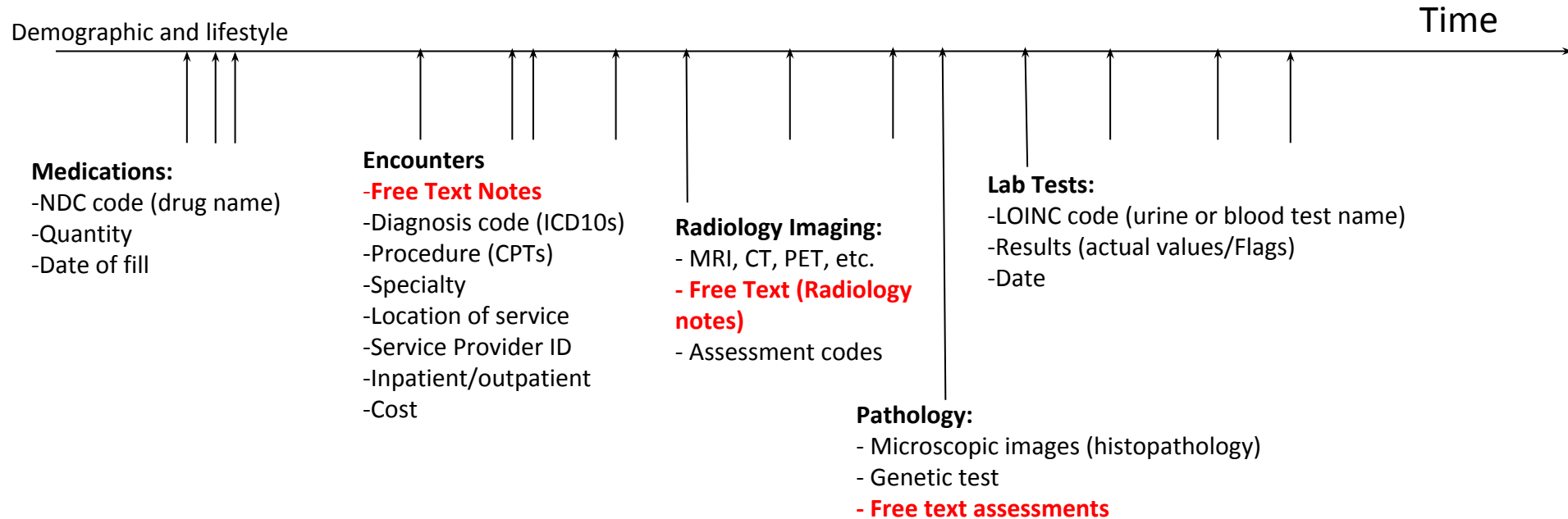
## Lab Tests:

- LOINC code (urine or blood test name)
- Results (actual values/Flags)
- Date

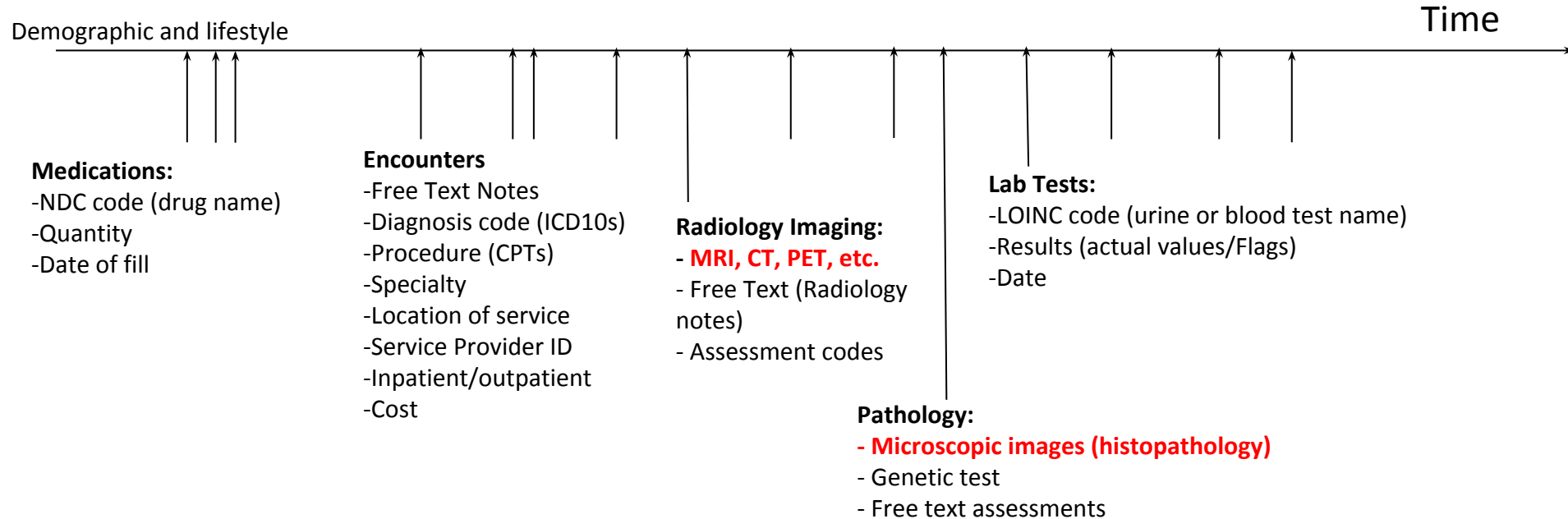




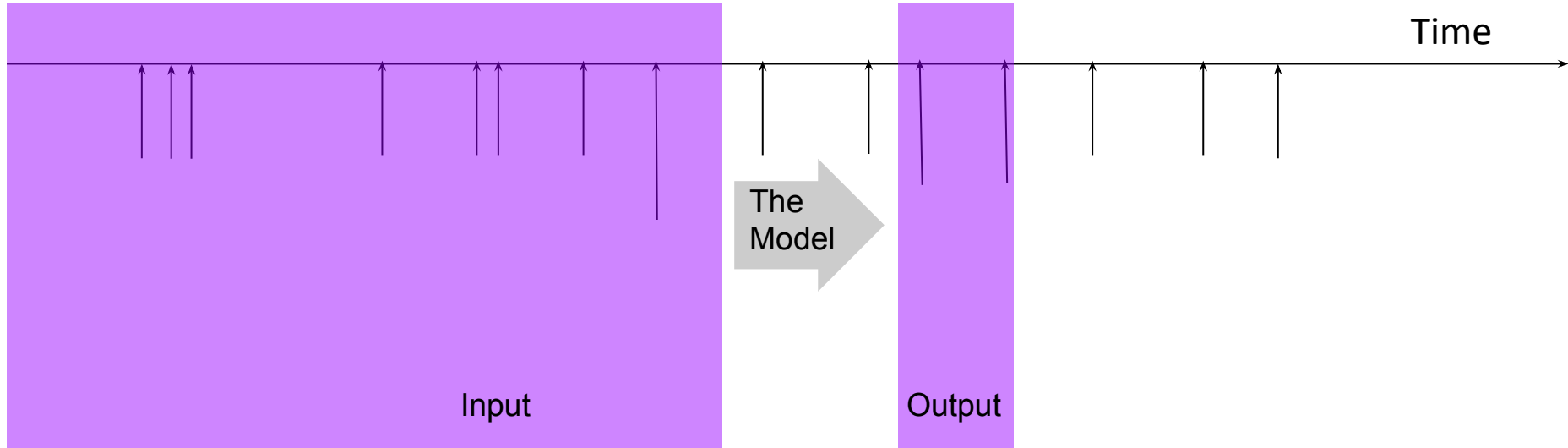
# Electronic Health Records



# Electronic Health Records



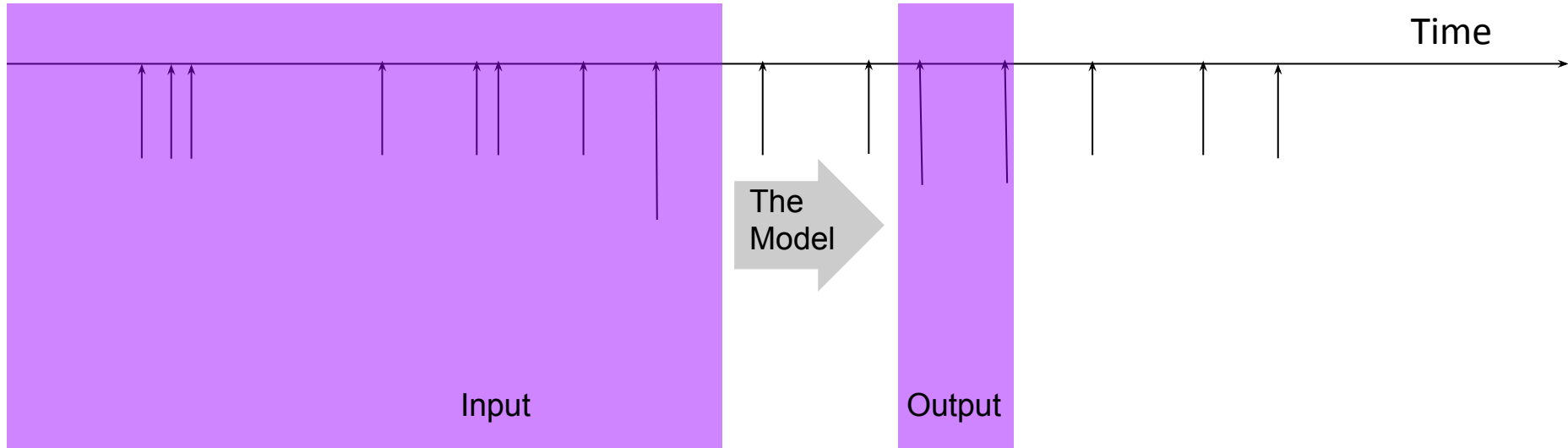
# Disease Prediction/Forecasting



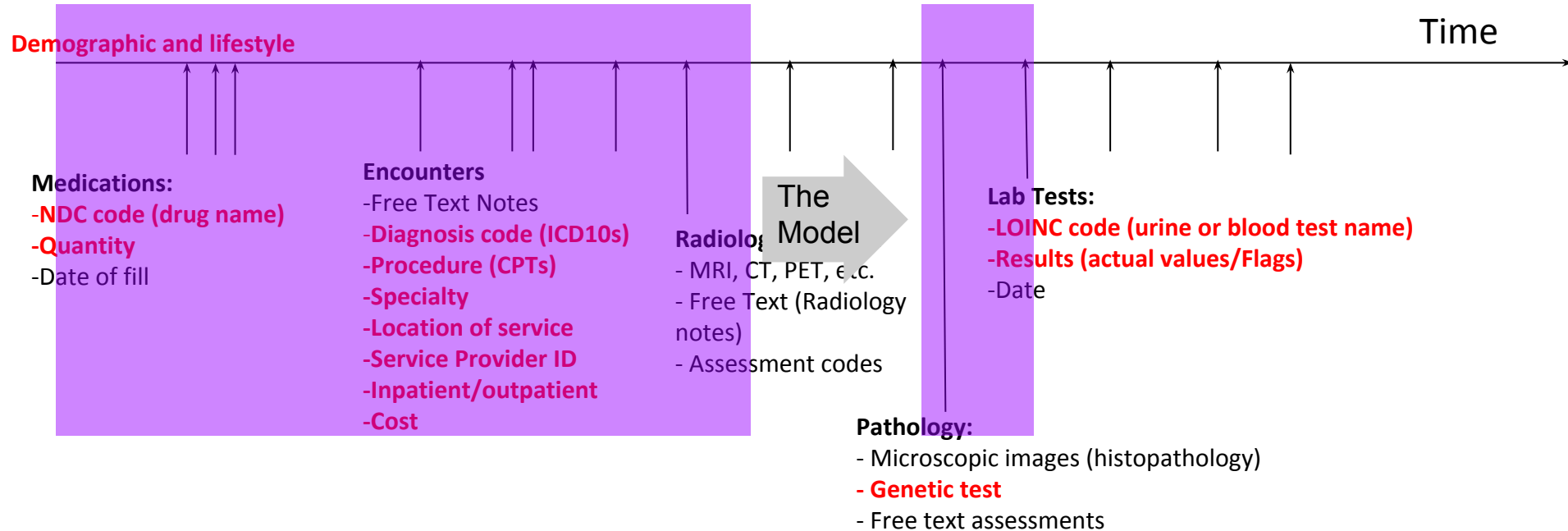
# Space of machine learning methods

|                  |                            | <i>Feature interactions</i>  |   |
|------------------|----------------------------|--|---|
|                  |                            | Specified by human experts   | +Learned  |
| Complex features | Specified by human experts | <ul style="list-style-type: none"><li>- Standard Regression</li><li>- Rule Based Expert Systems</li><li>- Bayesian networks</li></ul> <p><i>Parameters: Few</i><br/><i>Data Needed: Small</i></p>      | <ul style="list-style-type: none"><li>- Decision Trees</li><li>- Bayesian networks with structure learning</li><li>- Random Forests</li></ul> <p><i>Parameters: Medium</i><br/><i>Data Needed: Medium/large</i></p> |
|                  | +Learned                   | <ul style="list-style-type: none"><li>- Bayesian networks with hidden variables</li><li>- Dimensionality reduction - PCA/ICA</li></ul> <p><i>Parameters: Medium</i><br/><i>Data Needed: Medium</i></p> | <ul style="list-style-type: none"><li>- Deep learning</li></ul> <p><i>Parameters: Larges</i><br/><i>Data Needed: Large/X-Large</i></p>  |

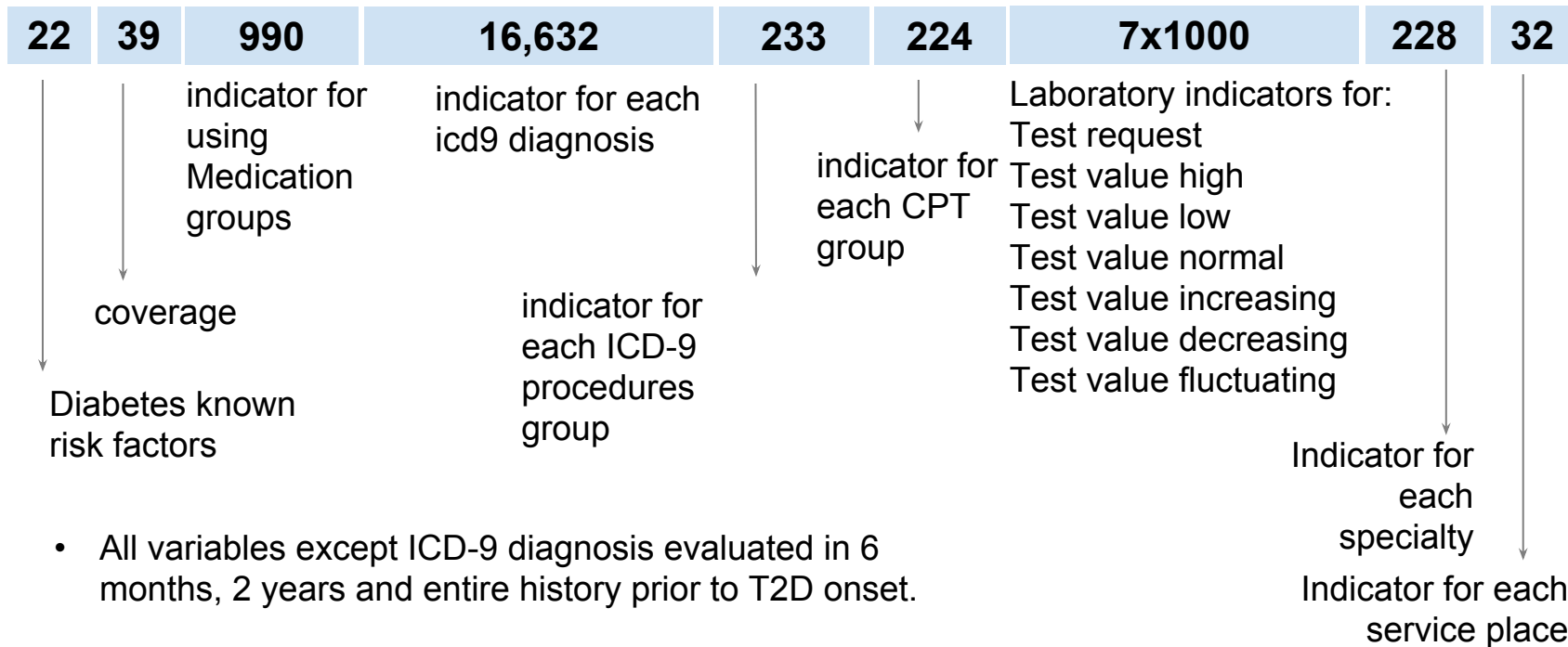
# Disease Prediction/Forecasting



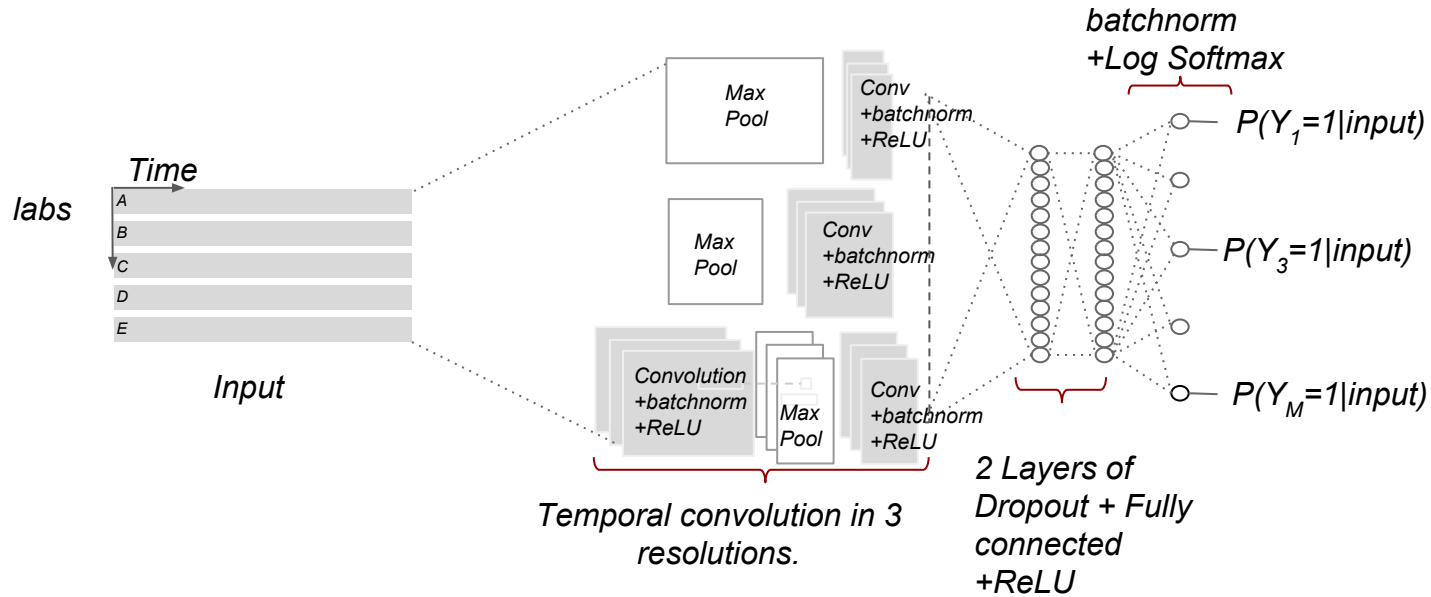
# Electronic Health Records



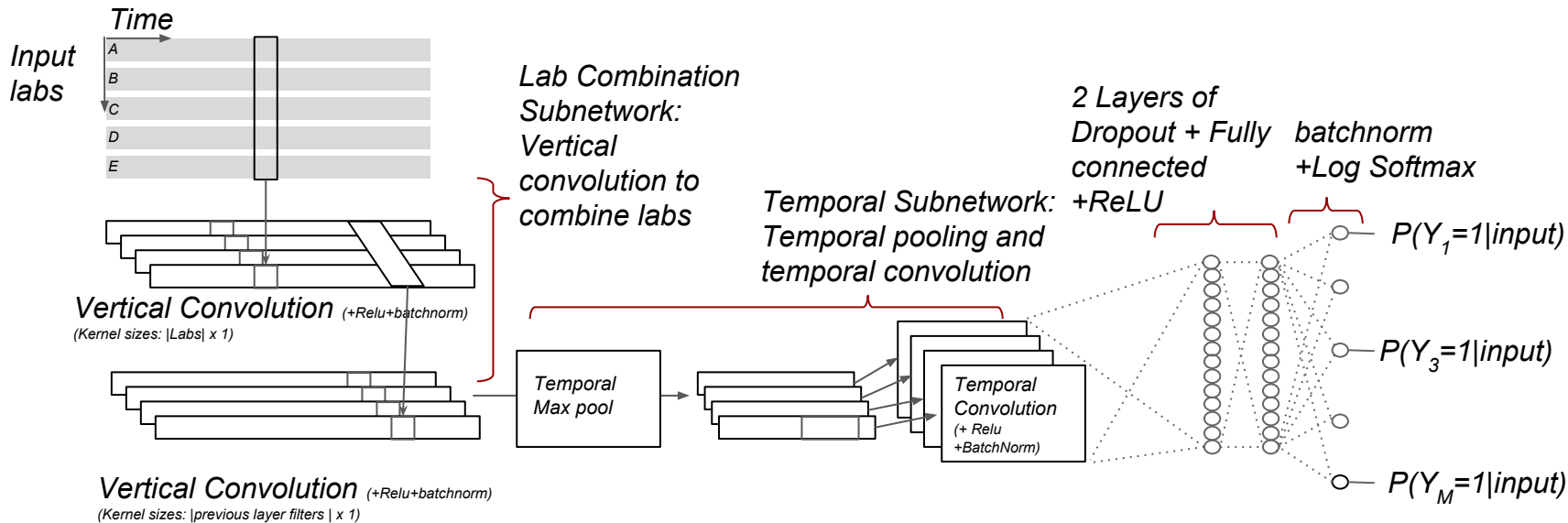
# Feature Engineering: ~42,000 features

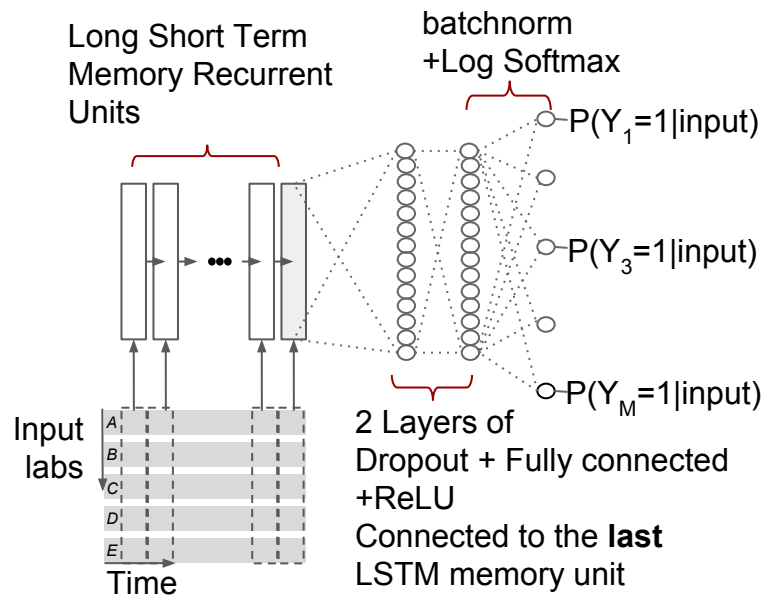


# Learning features and Deep Learning/Multitask learning





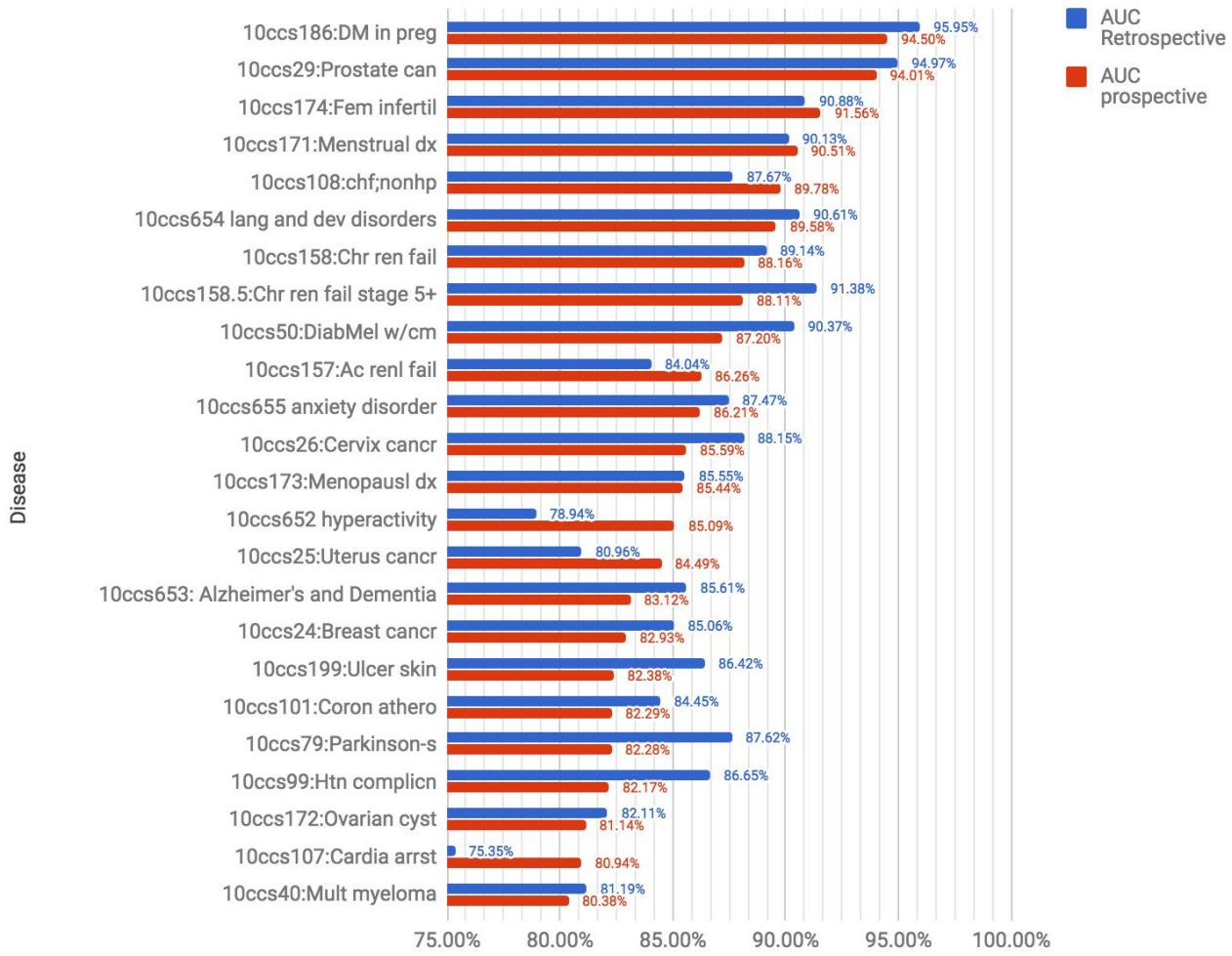




# Prediction Quality on the test set of size 98,000 individuals

| ICD9 Code and disease description      | LR    | LSTM  | CNN1  | CNN2  | Ens   | Pos  |
|--|-------|-------|-------|-------|-------|------|
| 585.6 End stage renal disease          | 0.886 | 0.917 | 0.910 | 0.916 | 0.920 | 837  |
| 285.21 Anemia in chr kidney dis        | 0.849 | 0.866 | 0.868 | 0.880 | 0.879 | 1598 |
| 585.3 Chr kidney dis stage III         | 0.846 | 0.851 | 0.857 | 0.858 | 0.864 | 2685 |
| 584.9 Acute kidney failure NOS         | 0.805 | 0.820 | 0.828 | 0.831 | 0.835 | 3039 |
| 250.01 DMI wo cmp nt st uncntrl        | 0.822 | 0.813 | 0.819 | 0.825 | 0.829 | 1522 |
| 250.02 DMII wo cmp uncntrld            | 0.814 | 0.819 | 0.814 | 0.821 | 0.828 | 3519 |
| 593.9 Renal and ureteral dis NOS       | 0.757 | 0.794 | 0.784 | 0.792 | 0.798 | 2111 |
| <b>428.0 CHF NOS</b>                   | 0.739 | 0.784 | 0.786 | 0.783 | 0.792 | 3479 |
| V053 Need prphyl vc vrl hepat          | 0.731 | 0.762 | 0.752 | 0.780 | 0.777 | 862  |
| <b>790.93 Elvtd prstate spcf antgn</b> | 0.666 | 0.758 | 0.761 | 0.768 | 0.772 | 1477 |
| <b>185 Malign neopl prostate</b>       | 0.627 | 0.757 | 0.751 | 0.761 | 0.768 | 761  |
| 274.9 Gout NOS                         | 0.746 | 0.761 | 0.764 | 0.757 | 0.767 | 1529 |
| <b>362.52 Exudative macular degen</b>  | 0.687 | 0.752 | 0.750 | 0.757 | 0.765 | 538  |
| <b>607.84 Impotence, organic orign</b> | 0.663 | 0.739 | 0.736 | 0.748 | 0.752 | 1372 |
| 511.9 Pleural effusion NOS             | 0.708 | 0.736 | 0.742 | 0.746 | 0.749 | 2701 |
| <b>616.10 Vaginitis NOS</b>            | 0.692 | 0.736 | 0.736 | 0.746 | 0.747 | 440  |
| <b>600.01 BPH w urinary obs/LUTS</b>   | 0.648 | 0.737 | 0.737 | 0.738 | 0.747 | 1681 |
| <b>285.29 Anemia-other chronic dis</b> | 0.672 | 0.713 | 0.725 | 0.746 | 0.739 | 1075 |
| <b>346.90 Migrne unsp wo ntrc mgrn</b> | 0.633 | 0.736 | 0.710 | 0.724 | 0.732 | 471  |
| 427.31 Atrial fibrillation             | 0.687 | 0.725 | 0.728 | 0.733 | 0.736 | 3766 |
| 250.00 DMII wo cmp nt st uncntr        | 0.708 | 0.718 | 0.708 | 0.719 | 0.728 | 3125 |
| 425.4 Prim cardiomyopathy NEC          | 0.683 | 0.718 | 0.719 | 0.722 | 0.726 | 1414 |
| 728.87 Muscle weakness-general         | 0.683 | 0.704 | 0.718 | 0.722 | 0.723 | 4706 |
| <b>620.2 Ovarian cyst NEC/NOS</b>      | 0.660 | 0.720 | 0.700 | 0.711 | 0.719 | 498  |
| 286.9 Coagulat defect NEC/NOS          | 0.690 | 0.694 | 0.709 | 0.715 | 0.718 | 958  |

# Overview of some results so far on *general* NYUMC patient cohort



# Applicable to many more outcomes and tasks

- Early prediction of childhood obesity
  - Predicting diabetes complications
  - Predicting risk of re-hospitalization
  - Detecting undocumented but existing diseases
  - Using lab values only to predict future diseases
  - Predicting medication adherence
  - Predicting no-shows
  - Etc. etc. etc....
- 
- Many industries interested: Hospitals, Insurance companies, Government Medicare/Medicaid, Center for Disease Control, etc.

# Medical Imaging:

Radiology (X-rays, Mammograms, MRI, Ultrasound)

Pathology

Microscopy

# Plain X-Rays or Radiographs

Most common & oldest type of radiology image.

Great to show *Carbon vs. Calcium*

Good for: Bones, Teeth, Chest X-Rays, Mammography, Abdominal X-ray.

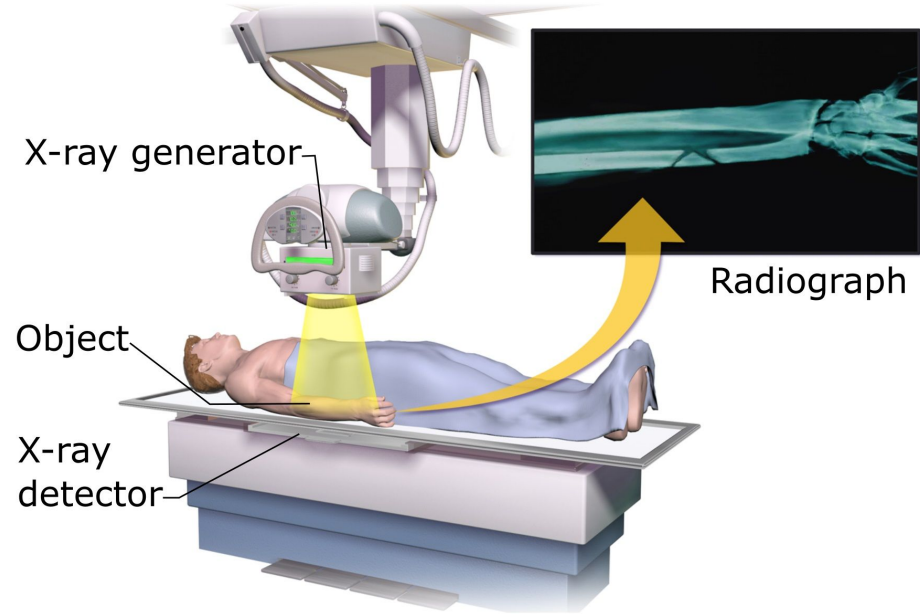
Result: 2D image

Risks: Radiation exposure

Opportunities in research:

- Augmented/automatic Diagnosis
- Lowering X-ray dosage

## Projectional radiography



# Related Papers on Bone X-Ray Radiographs

*MURA: Large Dataset for Abnormality Detection in Musculoskeletal Radiographs*

---

## **MURA: Large Dataset for Abnormality Detection in Musculoskeletal Radiographs**

---

**Pranav Rajpurkar<sup>1,\*</sup>, Jeremy Irvin<sup>1,\*</sup>, Aarti Bagul<sup>1</sup>, Daisy Ding<sup>1</sup>, Tony Duan<sup>1</sup>,  
Hershel Mehta<sup>1</sup>, Brandon Yang<sup>1</sup>, Kaylie Zhu<sup>1</sup>, Dillon Laird<sup>1</sup>, Robyn L. Ball<sup>2</sup>,  
Curtis Langlotz<sup>3</sup>, Katie Shpanskaya<sup>3</sup>, Matthew P. Lungren<sup>3,†</sup>, Andrew Y. Ng<sup>1,†</sup>**

\*,<sup>†</sup>Equal Contribution

<sup>1</sup>Department of Computer Science  
Stanford University  
{pranavsr, jirvin16}@cs.stanford.edu

<sup>2</sup>Department of Medicine  
Stanford University  
rball@stanford.edu

<sup>3</sup>Department of Radiology  
Stanford University  
mlungren@stanford.edu



# ***MURA: Large Dataset for Abnormality Detection in Musculoskeletal Radiographs***

Task: determining whether an X-ray study is normal or abnormal.

Motivation:

- Musculoskeletal conditions affect more than 1.7 billion people worldwide,
- 30 million emergency department visits annually

Data (Public):

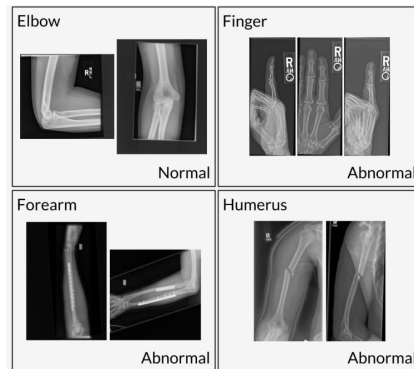
- 14,863 studies from 12,173 patients, with a total of 40,561 multi-view radiographic images.
- Includes: elbow, finger, forearm, hand, humerus, shoulder, and wrist
- Labels from Stanford Hospital (from 2001 to 2012)

Baseline:

- **DenseNet-169** with **Multi-task Cross Entropy Loss**

Evaluation:

- Cohen's kappa statistic



# MURA: Large Dataset for Abnormality Detection in Musculoskeletal Radiographs

## Leaderboard

Will your model perform as well as radiologists in detecting abnormalities in musculoskeletal X-rays?

| Rank | Date         | Model  | Kappa |
|------|--------------|--|-------|
|      |              | Best Radiologist Performance <i>Stanford University</i><br><i>Rajpurkar &amp; Irvin et al., 17</i>   | 0.778 |
| 1    | Aug 22, 2018 | base-comb3(ensemble) <i>jtz Availink</i>   | 0.805 |
| 2    | Sep 14, 2018 | double_res(ensemble model) <i>SCU_MILAB</i>  | 0.804 |
| 3    | Jul 24, 2018 | he_j   | 0.775 |
| 4    | Aug 19, 2018 | ianpan (ensemble) <i>RIH 3D Lab</i>  | 0.774 |
| 5    | Jul 24, 2018 | he_j   | 0.774 |
| 6    | Jun 17, 2018 | gcm (ensemble) <i>Peking University</i>  | 0.773 |
| 6    | Sep 10, 2018 | ty101 <i>single model</i>  | 0.773 |
| 7    | Aug 31, 2018 | he_j   | 0.764 |
| 7    | Aug 31, 2018 | AIAPlus (ensemble) <i>Taiwan AI Academy</i><br><a href="http://aiacademy.tw">http://aiacademy.tw</a> | 0.764 |
| 8    | Sep 04, 2018 | SER_Net_Baseline (single model) <i>SJTU</i>  | 0.764 |
| 9    | Jul 14, 2018 | Trs (single model) <i>SCU_MILAB</i>  | 0.763 |

# Related paper on Chest X-rays

## “ChestX-ray8: Hospital-scale Chest X-ray Database and Benchmarks on Weakly-Supervised Classification and Localization of Common Thorax Diseases”



This CVPR paper is the Open Access version, provided by the Computer Vision Foundation.  
Except for this watermark, it is identical to the version available on IEEE Xplore.

### ChestX-ray8: Hospital-scale Chest X-ray Database and Benchmarks on Weakly-Supervised Classification and Localization of Common Thorax Diseases

Xiaosong Wang<sup>1</sup>, Yifan Peng<sup>2</sup>, Le Lu<sup>1</sup>, Zhiyong Lu<sup>2</sup>, Mohammadhadi Bagheri<sup>1</sup>, Ronald M. Summers<sup>1</sup>

<sup>1</sup>Department of Radiology and Imaging Sciences, Clinical Center,

<sup>2</sup>National Center for Biotechnology Information, National Library of Medicine,  
National Institutes of Health, Bethesda, MD 20892

{xiaosong.wang,yifan.peng,le.lu,luzh,mohammad.bagheri,rms}@nih.gov

#### Abstract

*The chest X-ray is one of the most commonly accessible radiological examinations for screening and diagnosis of many lung diseases. A tremendous number of X-ray imaging studies accompanied by radiological reports are accumulated and stored in many modern hospitals' Picture Archiving and Communication Systems (PACS). On the other side, it is still an open question how this type of hospital-size knowledge database containing invaluable imaging informatics (i.e., loosely labeled) can be used to facilitate the data-hungry deep learning paradigms in building truly large-scale high precision computer-aided diagnosis (CAD) systems.*

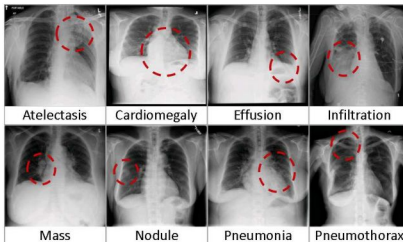


Figure 1. Eight common thoracic diseases observed in chest X-rays that validate a challenging task of fully-automated diagnosis.

# “ChestX-ray8: Hospital-scale Chest X-ray Database and Benchmarks on Weakly-Supervised Classification and Localization of Common Thorax Diseases”

Task: Identification & Localization of Thorax Diseases.

Motivation: Reducing medical errors and improving “incidental finding” success.

The data:

- 108,948 frontal view X-ray images of 32,717 unique patients
- Labels from radiology reports. (8 disease labels)

Evaluation: AUC

Baseline: Standard imaging models up to 2017

# “ChestX-ray8: Hospital-scale Chest X-ray Database and Benchmarks on Weakly-Supervised Classification and Localization of Common Thorax Diseases”

| Item #       | OpenI | Ov. | ChestX-ray8 | Ov.   |
|--------------|-------|-----|-------------|-------|
| Report       | 2,435 | -   | 108,948     | -     |
| Annotations  | 2,435 | -   | -           | -     |
| Atelectasis  | 315   | 122 | 5,789       | 3,286 |
| Cardiomegaly | 345   | 100 | 1,010       | 475   |
| Effusion     | 153   | 94  | 6,331       | 4,017 |
| Infiltration | 60    | 45  | 10,317      | 4,698 |
| Mass         | 15    | 4   | 6,046       | 3,432 |
| Nodule       | 106   | 18  | 1,971       | 1,041 |
| Pneumonia    | 40    | 15  | 1,062       | 703   |
| Pneumothorax | 22    | 11  | 2,793       | 1,403 |
| Normal       | 1,379 | 0   | 84,312      | 0     |

| Setting  | Atelectasis   | Cardiomegaly  | Effusion      | Infiltration  | Mass          | Nodule        | Pneumonia     | Pneumothorax  |
|--|---------------|---------------|---------------|---------------|---------------|---------------|---------------|---------------|
| Initialization with different pre-trained models |               |               |               |               |               |               |               |               |
| AlexNet  | 0.6458        | 0.6925        | 0.6642        | 0.6041        | <b>0.5644</b> | 0.6487        | 0.5493        | 0.7425        |
| GoogLeNet  | 0.6307        | 0.7056        | 0.6876        | 0.6088        | 0.5363        | 0.5579        | 0.5990        | 0.7824        |
| VGGNet-16  | 0.6281        | 0.7084        | 0.6502        | 0.5896        | 0.5103        | 0.6556        | 0.5100        | 0.7516        |
| ResNet-50  | <b>0.7069</b> | <b>0.8141</b> | <b>0.7362</b> | <b>0.6128</b> | 0.5609        | <b>0.7164</b> | <b>0.6333</b> | <b>0.7891</b> |
| Different multi-label loss functions             |               |               |               |               |               |               |               |               |
| CEL  | 0.7064        | 0.7262        | 0.7351        | 0.6084        | 0.5530        | 0.6545        | 0.5164        | 0.7665        |
| W-CEL  | 0.7069        | 0.8141        | 0.7362        | 0.6128        | 0.5609        | 0.7164        | 0.6333        | 0.7891        |

Table 3. AUCs of ROC curves for multi-label classification in different DCNN model setting.

| T(IoBB)  | Atelectasis | Cardiomegaly | Effusion | Infiltration | Mass   | Nodule | Pneumonia | Pneumothorax |
|--|-------------|--------------|----------|--------------|--------|--------|-----------|--------------|
| T(IoBB) = 0.1  |             |              |          |              |        |        |           |              |
| Acc.   | 0.7277      | 0.9931       | 0.7124   | 0.7886       | 0.4352 | 0.1645 | 0.7500    | 0.4591       |
| AFP  | 0.0823      | 0.0487       | 0.0589   | 0.0426       | 0.0691 | 0.0630 | 0.0691    | 0.0264       |
| T(IoBB) = 0.25 (Two times larger on both x and y axis than ground truth B-Boxes) |             |              |          |              |        |        |           |              |
| Acc.   | 0.5500      | 0.9794       | 0.5424   | 0.5772       | 0.2823 | 0.0506 | 0.5583    | 0.3469       |
| AFP  | 0.1666      | 0.1534       | 0.1189   | 0.0914       | 0.0975 | 0.0741 | 0.1250    | 0.0487       |
| T(IoBB) = 0.5  |             |              |          |              |        |        |           |              |
| Acc.   | 0.2833      | 0.8767       | 0.3333   | 0.4227       | 0.1411 | 0.0126 | 0.3833    | 0.1836       |
| AFP  | 0.2703      | 0.2611       | 0.1859   | 0.1422       | 0.1209 | 0.0772 | 0.1768    | 0.0772       |
| T(IoBB) = 0.75   |             |              |          |              |        |        |           |              |
| Acc.   | 0.1666      | 0.7260       | 0.2418   | 0.3252       | 0.1176 | 0.0126 | 0.2583    | 0.1020       |
| AFP  | 0.3048      | 0.3506       | 0.2113   | 0.1737       | 0.1310 | 0.0772 | 0.2184    | 0.0873       |
| T(IoBB) = 0.9  |             |              |          |              |        |        |           |              |
| Acc.   | 0.1333      | 0.6849       | 0.2091   | 0.2520       | 0.0588 | 0.0126 | 0.2416    | 0.0816       |
| AFP  | 0.3160      | 0.3983       | 0.2235   | 0.1910       | 0.1402 | 0.0772 | 0.2317    | 0.0904       |

Table 4. Pathology localization accuracy and average false positive number for 8 disease classes.

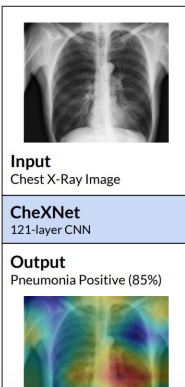
# Follow-up: CheXNet (Also a DenseNet model)

## CheXNet: Radiologist-Level Pneumonia Detection on Chest X-Rays with Deep Learning

Pranav Rajpurkar<sup>\*1</sup> Jeremy Irvin<sup>\*1</sup> Kaylie Zhu<sup>1</sup> Brandon Yang<sup>1</sup> Hershel Mehta<sup>1</sup>  
Tony Duan<sup>1</sup> Daisy Ding<sup>1</sup> Aarti Bagul<sup>1</sup> Robyn L. Ball<sup>2</sup> Curtis Langlotz<sup>3</sup> Katie Shpanskaya<sup>3</sup>  
Matthew P. Lungren<sup>3</sup> Andrew Y. Ng<sup>1</sup>

### Abstract

We develop an algorithm that can detect pneumonia from chest X-rays at a level exceeding practicing radiologists. Our algorithm, CheXNet, is a 121-layer convolutional neural network trained on ChestX-ray14, currently the largest publicly available chest X-ray dataset, containing over 100,000 frontal-view X-ray images with 14 diseases. Four practicing academic radiologists annotate a test set, on which we compare the performance of CheXNet to that of radiologists. We find that CheXNet exceeds average radiologist performance on the F1 metric. We extend CheXNet to detect all 14 diseases in ChestX-ray14 and achieve state of the art results on all 14 diseases.



### 1. Introduction

| Pathology          | Wang et al. (2017) | Yao et al. (2017) | CheXNet (ours) |
|--------------------|--------------------|-------------------|----------------|
| Atelectasis        | 0.716              | 0.772             | <b>0.8094</b>  |
| Cardiomegaly       | 0.807              | 0.904             | <b>0.9248</b>  |
| Effusion           | 0.784              | 0.859             | <b>0.8638</b>  |
| Infiltration       | 0.609              | 0.695             | <b>0.7345</b>  |
| Mass               | 0.706              | 0.792             | <b>0.8676</b>  |
| Nodule             | 0.671              | 0.717             | <b>0.7802</b>  |
| Pneumonia          | 0.633              | 0.713             | <b>0.7680</b>  |
| Pneumothorax       | 0.806              | 0.841             | <b>0.8887</b>  |
| Consolidation      | 0.708              | 0.788             | <b>0.7901</b>  |
| Edema              | 0.835              | 0.882             | <b>0.8878</b>  |
| Emphysema          | 0.815              | 0.829             | <b>0.9371</b>  |
| Fibrosis           | 0.769              | 0.767             | <b>0.8047</b>  |
| Pleural Thickening | 0.708              | 0.765             | <b>0.8062</b>  |
| Hernia             | 0.767              | 0.914             | <b>0.9164</b>  |

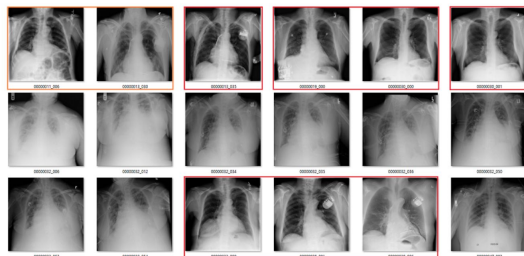
|                  | F1 Score (95% CI)    |
|------------------|----------------------|
| Radiologist 1    | 0.383 (0.309, 0.453) |
| Radiologist 2    | 0.356 (0.282, 0.428) |
| Radiologist 3    | 0.365 (0.291, 0.435) |
| Radiologist 4    | 0.442 (0.390, 0.492) |
| Radiologist Avg. | 0.387 (0.330, 0.442) |
| CheXNet          | 0.435 (0.387, 0.481) |

# Criticism of the Dataset (Applies to most datasets)

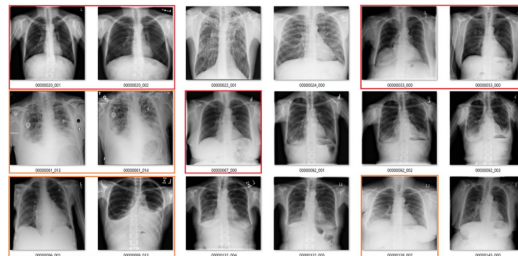
## Labels aren't accurate

In all the images, red = clearly wrong label. Orange = I doubt it, I wouldn't report it, but I can't really exclude it. Correlate clinically :p

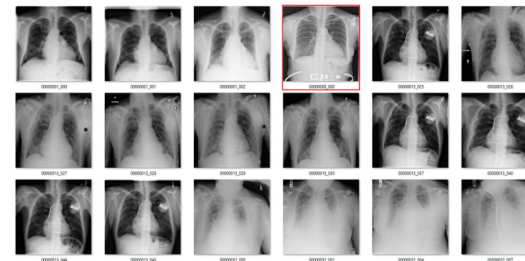
Atelectasis



Fibrosis



Cardiomegaly



Read: <https://lukeoakdenrayner.wordpress.com/2017/12/18/the-chestxray14-dataset-problems/>

# Mammograms: Low-dose X-Rays

Screening Mammograms: 4 images  
Diagnostic Mammograms: More than  
4 images

Currently recommended once every 2  
years for every 50-74 yo women.

Does not work for dense breasts.  
(Many young patients or asian  
ethnicities)

- Ultrasound





# Related paper on automatic Mammography Screening

1

## High-Resolution Breast Cancer Screening with Multi-View Deep Convolutional Neural Networks

Krzysztof J. Geras<sup>1,3</sup>, Stacey Wolfson<sup>3</sup>, Yiqiu Shen<sup>1</sup>, Nan Wu<sup>1</sup>, S. Gene Kim<sup>3,4</sup>, Eric Kim<sup>3</sup>,  
Laura Heacock<sup>3</sup>, Ujas Parikh<sup>3</sup>, Linda Moy<sup>3,4</sup>, Kyunghyun Cho<sup>1,2,5</sup>

*Abstract*—Advances in deep learning for natural images have prompted a surge of interest in applying similar techniques to medical images. The majority of the initial attempts focused on replacing the input of a deep convolutional neural network with a medical image, which does not take into consideration the fundamental differences between these two types of images. Specifically, fine details are necessary for detection in medical images, unlike in natural images where coarse structures matter most. This difference makes it inadequate to use the existing network architectures developed for natural images, because they work on heavily downsampled images to reduce the memory requirements. This hides details necessary to make accurate predictions. Additionally, a single exam in medical imaging often comes with a set of views which must be fused in order to reach a correct conclusion. In our work, we propose to use a multi-view deep convolutional neural network that handles a set of high-resolution medical images. We evaluate it on large-scale mammography-based breast cancer screening (BI-RADS prediction) using 886,000 images. We focus on investigating the impact of the training set size and image size on the prediction accuracy. Our results highlight that performance increases with the size of training set, and that the best performance can only be achieved using the original resolution. In the reader study, performed on a random subset of the test set, we confirmed the efficacy of our model, which achieved performance comparable to a committee of radiologists when presented with the same data.

*Index Terms*—breast cancer screening, deep convolutional neural networks, deep learning, machine learning, mammography

screening interval for mammograms has been the subject of public debate with different professional societies offering varying guidelines for mammographic screening [2], [3], [4], [5]. In particular, there has been public discussion regarding the potential harms of screening. These harms include false positive recalls and false positive biopsies as well as anxiety caused by recall for diagnostic testing after a screening exam. Overall, the recall rate following a screening mammogram is between 10-15%. This equates to about 3.3 to 4.5 million callback exams for additional testing [6].

The vast majority of the women asked to return following an inconclusive mammogram undergo another mammogram and/or ultrasound for clarification. Most of these false positive findings are found to represent normal breast tissue. Only 10% to 20% of women who have an abnormal screening mammogram are recommended to undergo a biopsy. Only 20-40% of these biopsies yield a diagnosis of cancer [7]. In 2014, over 39 million screening and diagnostic mammography exams were performed in the US. Therefore, in addition to the anxiety from undergoing a false positive mammogram, there are significant costs associated with unnecessary follow ups and biopsies. Clearly, there is an unmet need to shift the balance of routine breast cancer screening towards more benefit and less harm.

03.07047v3 [cs.CV] 28 Jun 2018

# High-Resolution Breast Cancer Screening with Multi-View Deep Convolutional Neural Networks

Data: 886,000 images, 129,208 unique patients

|            | BI-RADS 0     | BI-RADS 1      | BI-RADS 2      |
|------------|---------------|----------------|----------------|
| Training   | 21946 / 95471 | 74832 / 327035 | 67446 / 298680 |
| Validation | 2634 / 11471  | 11542 / 50627  | 10376 / 46178  |
| Test       | 1341 / 5871   | 5986 / 26213   | 5595 / 24891   |

Labels: BI-RADs scores

Baseline: Custom CNN

Evaluation: AUC & Reader Study

|              | radiologists | MV-DCN | radiologists + MV-DCN |
|--------------|--------------|--------|-----------------------|
| 0 vs. others | 0.650        | 0.547  | 0.653                 |
| 1 vs. others | 0.765        | 0.757  | 0.792                 |
| 2 vs. others | 0.699        | 0.759  | 0.759                 |
| macAUC       | 0.704        | 0.688  | 0.735                 |

| layer                  | kernel size | stride | #maps | repetition |
|------------------------|-------------|--------|-------|------------|
| global average pooling |             |        | 256   |            |
| convolution            | 3×3         | 1×1    | 256   | ×3         |
| max pooling            | 2×2         | 2×2    | 128   |            |
| convolution            | 3×3         | 1×1    | 128   | ×3         |
| max pooling            | 2×2         | 2×2    | 128   |            |
| convolution            | 3×3         | 1×1    | 128   | ×3         |
| max pooling            | 2×2         | 2×2    | 64    |            |
| convolution            | 3×3         | 1×1    | 64    | ×2         |
| convolution            | 3×3         | 2×2    | 64    |            |
| max pooling            | 3×3         | 3×3    | 32    |            |
| convolution            | 3×3         | 2×2    | 32    |            |
| input                  |             |        | 1     |            |

Fig. 2. Description of one deep convolutional network column for a single view. It transforms the input view (a gray-scale image) into a 256-dimensional vector.

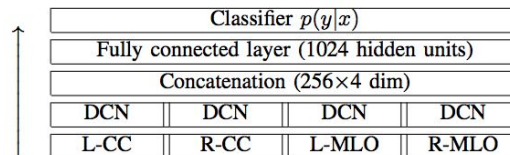


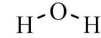
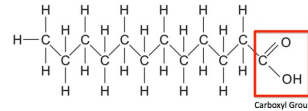
Fig. 3. An overview of the proposed multi-view deep convolutional network. DCN refers to the convolutional network network column from Figure 2. The arrow indicates the direction of information flow.

# Magnetic Resonance Imaging (MRI)

Watch (25 mins): [https://www.youtube.com/watch?v=djAxjtN\\_7VE](https://www.youtube.com/watch?v=djAxjtN_7VE)

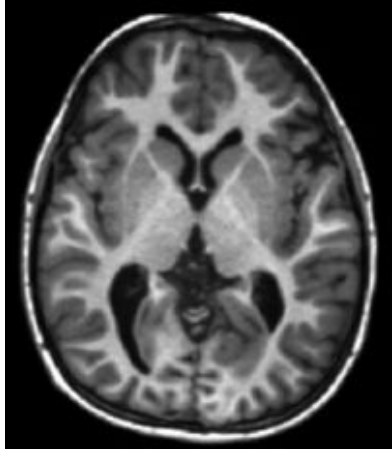
- Protons (Hydrogen nuclei) rotate randomly.
- A rotating positive charge creates magnetic field.
- If put under a bigger magnetic field, the proton spins somewhat lines-up.
- If exposed to radio-frequency proportional to the magnetic field, they flip.
- As the radio-frequency is removed, they emit a measurable signal (Phase & Frequency & Magnitude) as they go back.

- **Fat** has different reaction to this removal vs **Water**

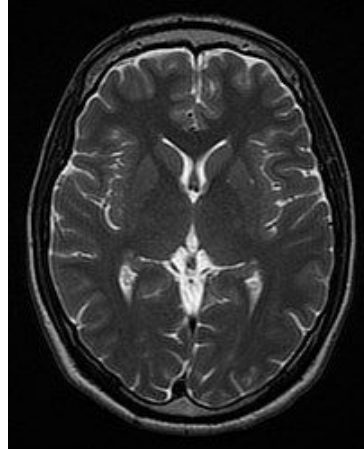


- **Pulse Sequence:** Order of applying and removing radio-frequency.
- Can localize each measured signal by creating asymmetric large magnetic waves.
- MRI signal is originally captured in Fourier Space
- Currently 1.5 T, 3 T, 7 Tesla clinically available.

# Pulse Sequences: T1 vs T2 vs FLAIR vs DTI vs ...



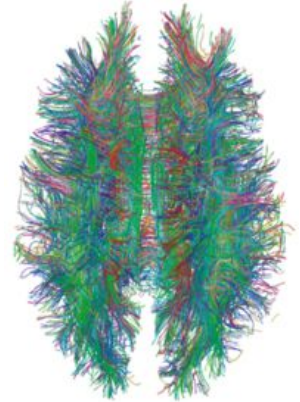
**T1:**  
Brighter: Fat and Contrast agents  
Darker: Higher water content: (edema, tumor, infarction, inflammation, infection, hemorrhage)



**T2:**  
Brighter: Water  
Darker: Fat tissue

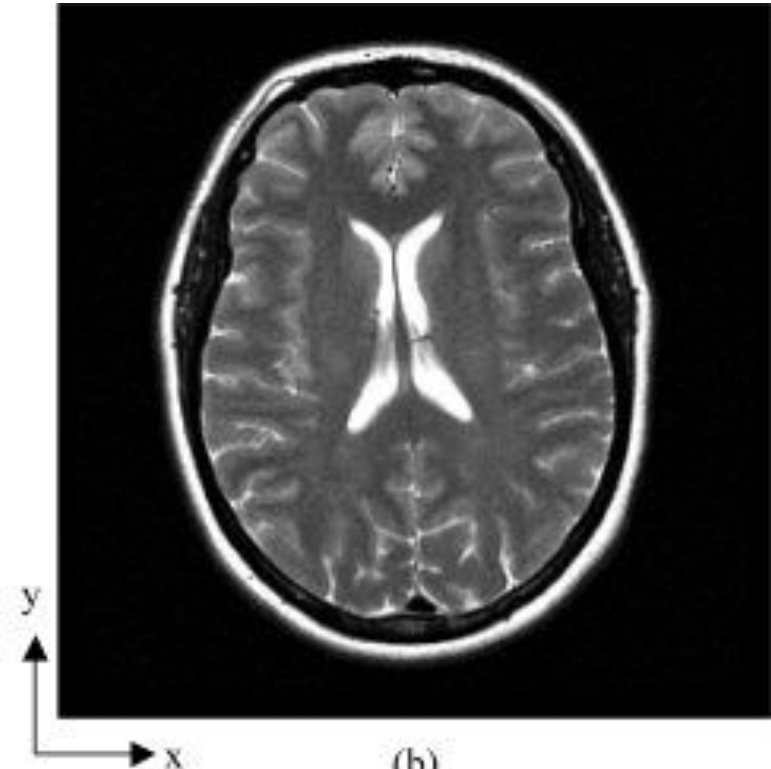
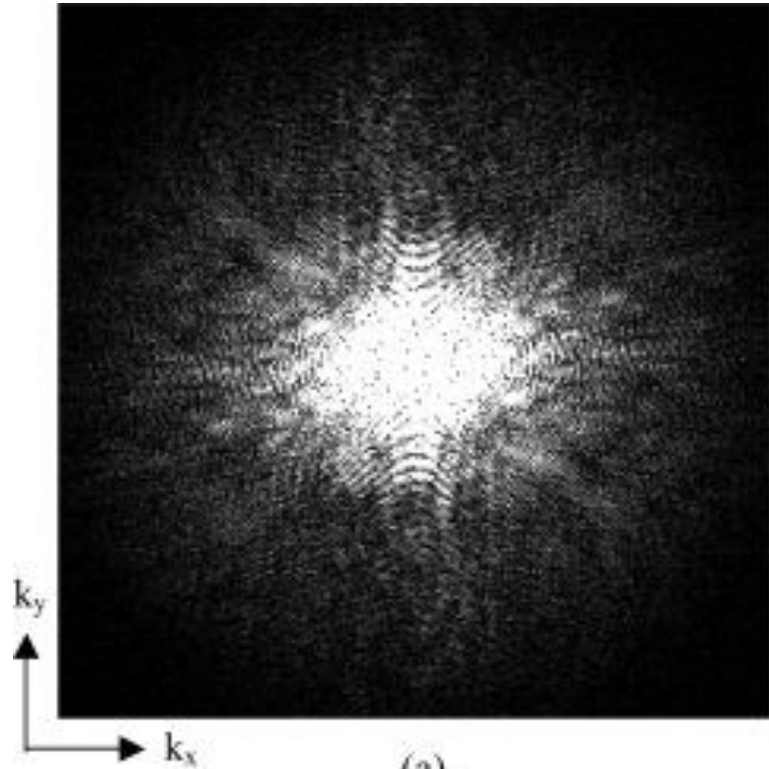


**FLAIR:** High signal in stroke, multiple sclerosis (MS) plaques, subarachnoid haemorrhage and meningitis.

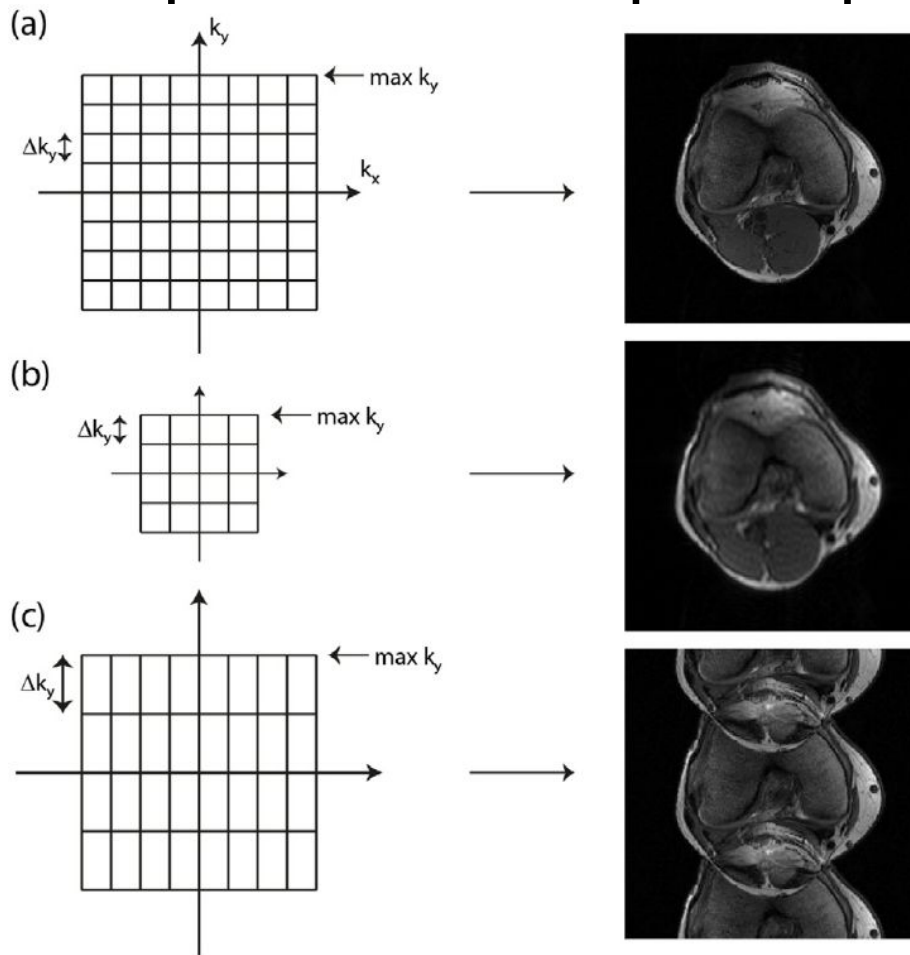


**DTI:**  
Measures of Brownian motion of water molecules  
Can image direction of nerve fibers  
Useful for tumor deformation studies

MRI is originally in **Fourier Space** - called K-Space



# Missing data in K-space leads to pixel space artifacts



# Issues and Potentials for Research

## Improving Acquisition time & Image reconstruction

15/20 minutes stuck inside a tube: too long!

## Diagnosis and automation:

2D and 3D classifiers, localization, segmentation

Time series alignment, classification, visualization

## Advanced Imaging Invention

MRI fingerprinting and diagnosis

# Segmentation of MRIs: Brain

“QuickNAT: Segmenting MRI Neuroanatomy in 20 seconds”

## **QuickNAT: Segmenting MRI Neuroanatomy in 20 seconds**

Abhijit Guha Roy, Sailesh Conjeti, Nassir Navab and Christian Wachinger

### Affiliations:

A. Guha Roy, C. Wachinger

Laboratory for Artificial Intelligence in Medical Imaging (AI-Med),  
Department of Child and Adolescent Psychiatry, Psychosomatic and  
Psychotherapy,  
Ludwig-Maximilian-University,  
Waltherstr. 23, 80337 Munich, Germany

A. Guha Roy, S. Conjeti, N. Navab

Chair for Computer Aided Medical Procedures, Department of Informatics  
Technical University of Munich,  
Boltzmannstr. 3, 85748 Garching, Munich, Germany.

S. Conjeti

German Center for Neurodegenerative Diseases (DZNE)



# “QuickNAT: Segmenting MRI Neuroanatomy in 20 seconds”

Motivation:

- Accurate brain structural segmentation is central to nearly all neuroimaging analyses.
- Freesurfer takes 2-4 hours to segment a volume.

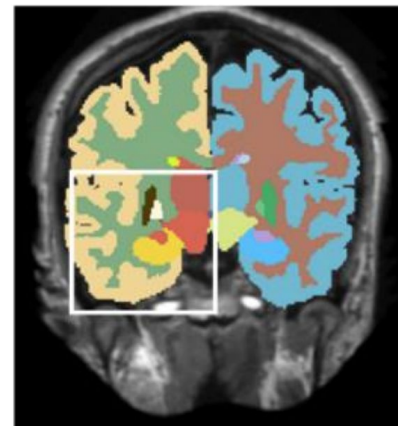
Task: Segmentation of 40+ regions per volume

Data: ADNI Auxiliary data & MICCAI brain segmentation challenge (30 manual segmented volumes)

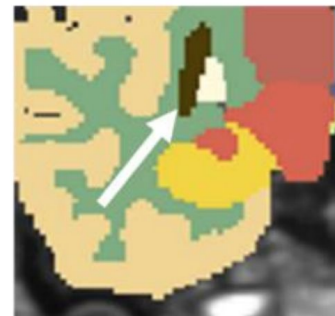
Baseline: Variant of U-net

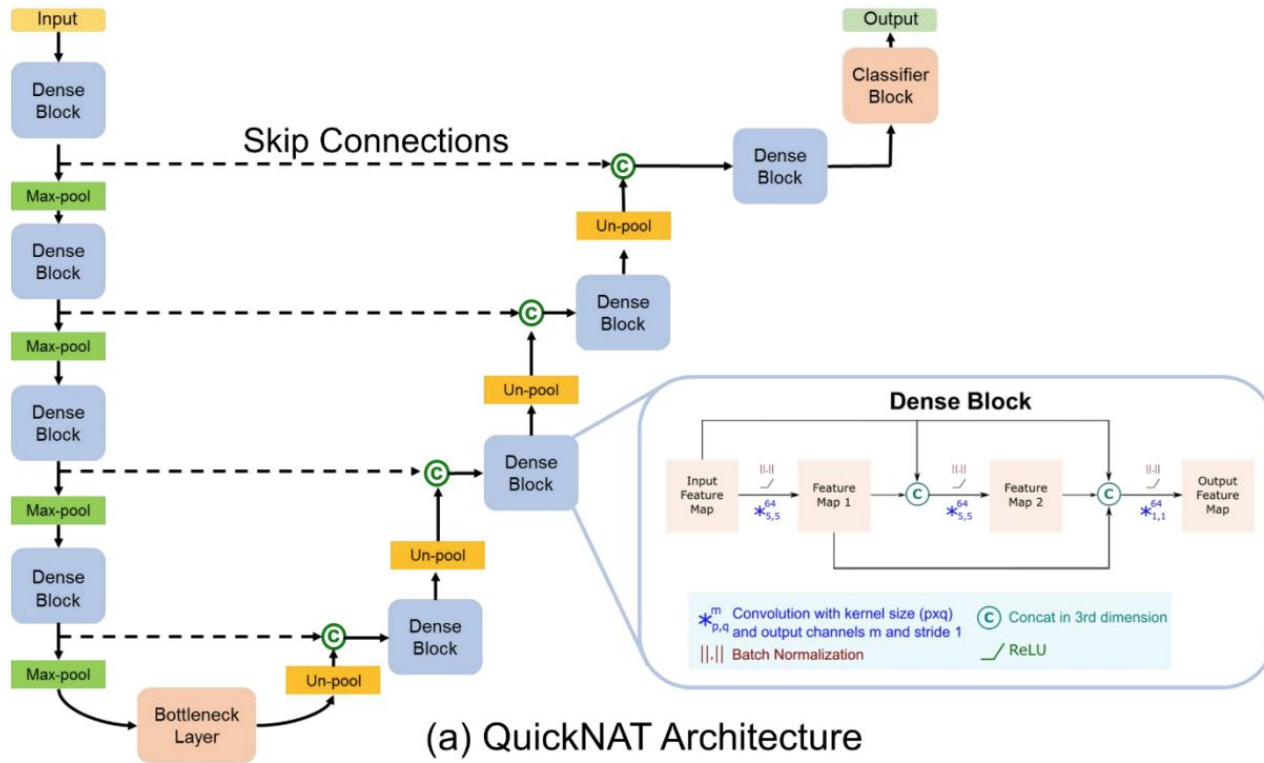
Loss function: Weighted cross entropy & Weighted Dice

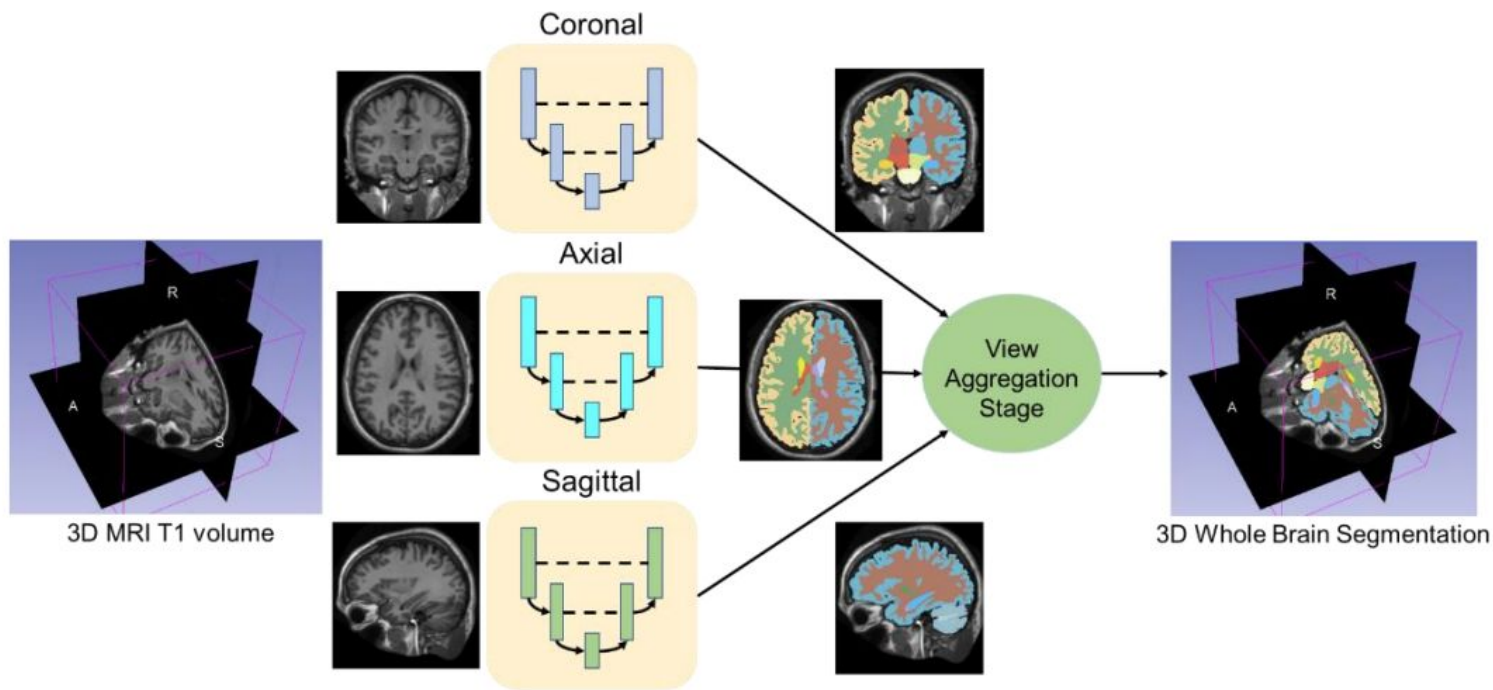
$$\text{loss}_{Dice} = \frac{2 \cdot |\text{mask} \cap \text{prediction}|}{|\text{mask}| + |\text{prediction}|}$$



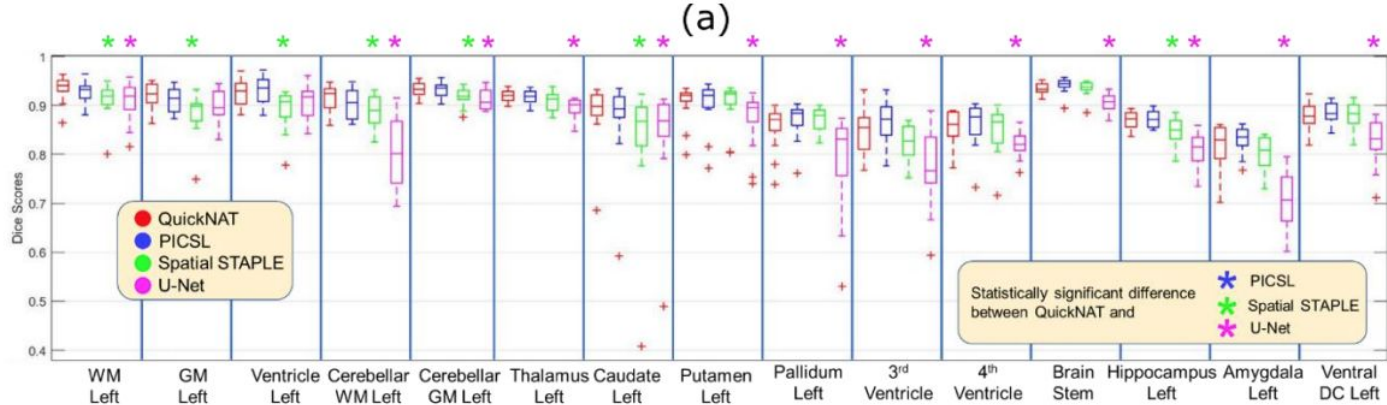
(i) Ground Truth



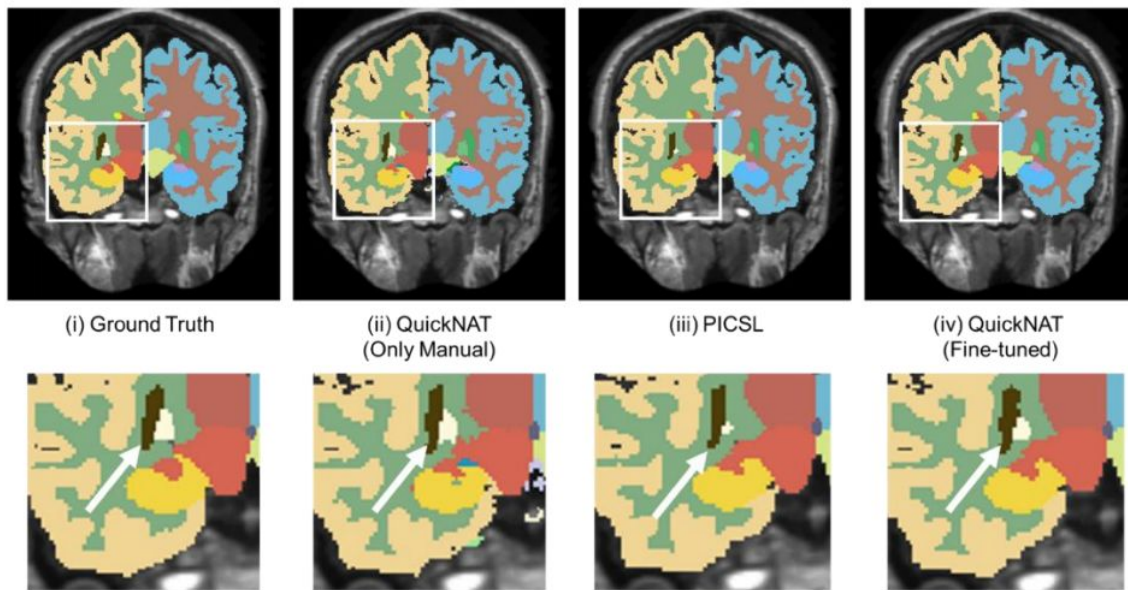




(b) Multi-View Aggregation  
for final prediction



(b)



# “End-To-End Alzheimer’s Disease Diagnosis and Biomarker Identification”

<https://arxiv.org/pdf/1810.00523.pdf>

## End-To-End Alzheimer’s Disease Diagnosis and Biomarker Identification

Soheil Esmaeilzadeh<sup>1</sup>, Dimitrios Ioannis Belivanis<sup>1</sup>,  
Kilian M. Pohl<sup>2</sup>, and Ehsan Adeli<sup>1</sup>

<sup>1</sup>Stanford University    <sup>2</sup>SRI International  
{soes, dbelivan, eadeli}@stanford.edu    kilian.pohl@sri.com

**Abstract.** As shown in computer vision, the power of deep learning lies in automatically learning relevant and powerful features for any perception task, which is made possible through end-to-end architectures. However, deep learning approaches applied for classifying medical images do not adhere to this architecture as they rely on several pre- and post-processing steps. This shortcoming can be explained by the relatively small number of available labeled subjects, the high dimensionality of neuroimaging data, and difficulties in interpreting the results of deep learning methods. In this paper, we propose a simple 3D Convolutional Neural Networks and exploit its model parameters to tailor the end-to-end architecture for the diagnosis of Alzheimer’s disease (AD). Our model can diagnose AD with an accuracy of 94.1% on the popular ADNI dataset using only MRI data, which outperforms the previous state-of-the-art. Based on the learned model, we identify the disease biomarkers, the results of which were in accordance with the literature. We further transfer the learned model to diagnose mild cognitive impairment (MCI), the prodromal stage of AD, which yield better results compared to other methods.

v1 [cs.CV] 1 Oct 2018

# “End-To-End Alzheimer’s Disease Diagnosis and Biomarker Identification”

Task: Differentiate between AD, MCI, Normal

Dataset: ADNI (publicly available) - small-ish

Table 1: ADNI-1 subjects demographic information.

| Class | Sex | Count | Age      |      |      |      |      |      |
|-------|-----|-------|----------|------|------|------|------|------|
|       |     |       | mean±std | min  | 25%  | 50%  | 75%  | max  |
| AD    | M   | 97    | 75.0±7.9 | 55.2 | 70.8 | 75.3 | 80.4 | 91.0 |
|       | F   | 103   | 76.1±7.4 | 56.5 | 71.1 | 77.0 | 82.3 | 87.9 |
| MCI   | M   | 265   | 75.4±7.3 | 54.6 | 71.0 | 75.4 | 80.7 | 89.8 |
|       | F   | 146   | 73.6±7.5 | 55.2 | 69.1 | 74.3 | 79.7 | 86.2 |
| NC    | M   | 112   | 76.1±4.7 | 62.2 | 72.5 | 75.8 | 78.5 | 89.7 |
|       | F   | 118   | 75.8±5.2 | 60.0 | 72.1 | 75.6 | 79.1 | 87.7 |

Architecture: 3D CNN - vanilla 3D

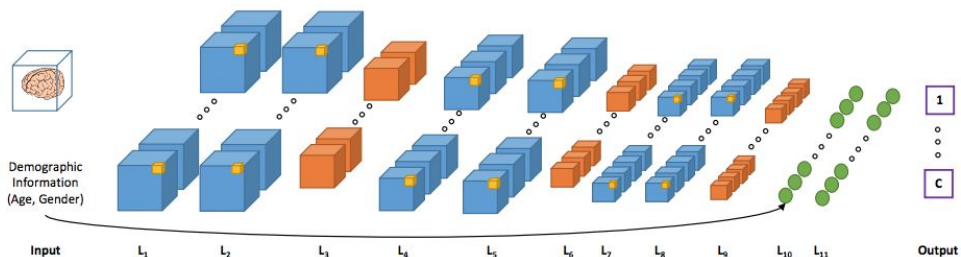


Fig. 2: 3D-CNN architecture used in this paper. The blue cubes ( $L_1$ ,  $L_2$ ,  $L_4$ ,  $L_5$ ,  $L_7$ , and  $L_8$ ) are convolutional layers; Orange cubes ( $L_3$ ,  $L_6$ , and  $L_9$ ) are max-pooling layers; and the last two layers are fully connected (FC) layers.

# Results & Visualizations

Table 2: Ablation tests: testing performance comparison of different models (last row is our model). The comparison includes the Accuracy (Acc),  $F_2$  score, Precision (Pre), and Recall (Rec) of all methods (Reg: Regularization, D/O: Drop-Out, Aug: Augmentation).

| Model                     | Simple      |             |             |             | Complex |       |      |      |
|---------------------------|-------------|-------------|-------------|-------------|---------|-------|------|------|
|                           | Acc%        | $F_2$       | Pre         | Rec         | Acc%    | $F_2$ | Pre  | Rec  |
| 3D-CNN                    | 68.7        | 0.71        | 0.68        | 0.72        | 66.5    | 0.69  | 0.67 | 0.70 |
| 3D-CNN+Reg                | 77.6        | 0.77        | 0.74        | 0.78        | 77.4    | 0.75  | 0.72 | 0.76 |
| 3D-CNN+Reg+D/O            | 83.1        | 0.811       | 0.78        | 0.82        | 79.7    | 0.82  | 0.79 | 0.84 |
| 3D-CNN+Reg+D/O+Aug (Ours) | <b>94.1</b> | <b>0.93</b> | <b>0.92</b> | <b>0.94</b> | 88.3    | 0.89  | 0.88 | 0.91 |

Table 3: Comparisons with prior works for AD diagnosis.

| Method | Modalities | Acc%        | Sen  | Spe  |
|--------|------------|-------------|------|------|
| [12]   | MRI+PET    | 85.7        | 0.99 | 0.54 |
| [3]    | MRI        | 90.8        | N/A  | N/A  |
| [10]   | MRI        | 91.1        | 0.88 | 0.93 |
| [5]    | MRI        | 93.9        | 0.94 | 0.93 |
| Ours   | MRI        | <b>94.1</b> | 0.94 | 0.91 |

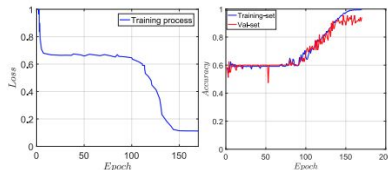


Fig. 3: (Left) training loss and (Right) training-validation accuracies with respect to the number of epochs for our 3D-CNN.

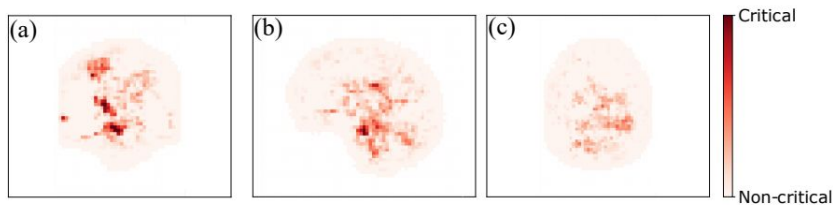


Fig. 4: Relative importance of different voxels associated with AD diagnosis.

Table 4: Testing performance for three-class Alzheimer classification.

| Method                                | Simple      |             |             |             | Complex |       |      |      |
|---------------------------------------|-------------|-------------|-------------|-------------|---------|-------|------|------|
|                                       | Acc%        | $F_2$       | Pre         | Rec         | Acc%    | $F_2$ | Pre  | Rec  |
| 3D-CNN+D/O+Reg+with learning transfer | <b>61.1</b> | <b>0.62</b> | <b>0.59</b> | <b>0.63</b> | 57.2    | 0.59  | 0.55 | 0.61 |
| 3D-CNN+D/O+Reg+w/o learning transfer  | 0.54        | 0.53.4      | 0.49        | 0.55        | 48.3    | 0.50  | 0.45 | 0.52 |

# Ultrasound Imaging or Sonography

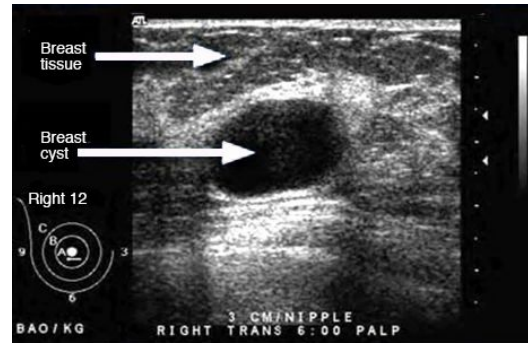
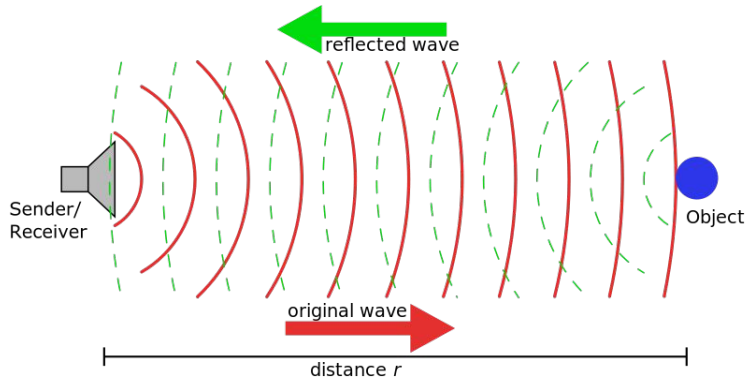
Sound waves with frequencies - higher than those audible to humans (>20,000 Hz)

provides images in real-time

No radiation and portable

Limits on its field of view: Difficult to 'see' behind Bones and Air (for now)

Can be used to see: Elasticity of tissue, 3D shape, Tissue maps



© MAYO FOUNDATION FOR MEDICAL EDUCATION AND RESEARCH. ALL RIGHTS RESERVED.





# “Automated and real-time segmentation of suspicious breast masses using convolutional neural network”

Motivation: Detection and Localization of tumors

Model: Standard U-Net

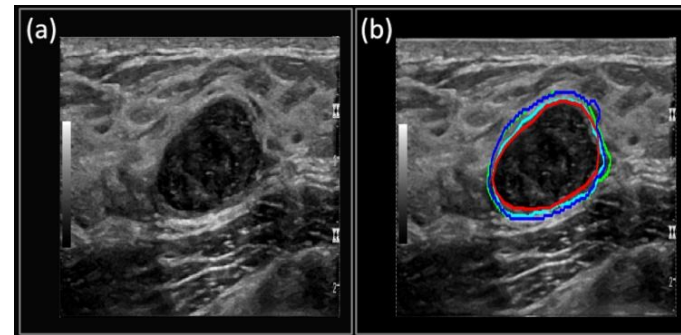
Data:

BI-RADS distribution of patients in training/validation and test sets.

| BI-RADS | No. of Patients in Training and Validation Set | No. of Patients in Testing Set |
|---------|--|--------------------------------|
| 2       | 3  | 1                              |
| 3       | 2  | 10                             |
| 4       | 155  | 35                             |
| 5       | 41   | 15                             |
| 6       | 6  | 0                              |

Evaluation: Dice Loss

| Metrics          |      | All cases (n = 61) | Benign (n = 39) | Malignant (n = 22) | IDC (n = 14) | Fibroadenoma (n = 23) |
|------------------|------|--------------------|-----------------|--------------------|--------------|-----------------------|
| Dice coefficient | MU   | 0.82±0.10          | 0.81±0.11       | 0.83±0.09          | 0.81±0.10    | 0.84±0.09             |
|                  | DRLS | 0.84±0.09          | 0.82±0.10       | 0.87±0.07          | 0.87±0.06    | 0.84±0.06             |
|                  | OU   | 0.52±0.27          | 0.48±0.28       | 0.57±0.24          | 0.55±0.28    | 0.48±0.27             |
| TPF <sup>a</sup> | MU   | 0.84±0.15          | 0.80±0.16       | 0.89±0.11          | 0.90±0.13    | 0.80±0.14             |
|                  | DRLS | 0.79±0.12          | 0.76±0.12       | 0.83±0.12          | 0.83±0.12    | 0.77±0.10             |
|                  | OU   | 0.61±0.06          | 0.55±0.06       | 0.70±0.05          | 0.68±0.07    | 0.57±0.04             |
| FPF <sup>b</sup> | MU   | 0.01±0.02          | 0.01±0.02       | 0.02±0.02          | 0.02±0.02    | 0.01±0.01             |
|                  | DRLS | 0.01±0.02          | 0.01±0.02       | 0.01±0.02          | 0.01±0.02    | 0.01±0.01             |
|                  | OU   | 0.31±0.06          | 0.31±0.05       | 0.27±0.07          | 0.29±0.09    | 0.32±0.04             |



Pathology

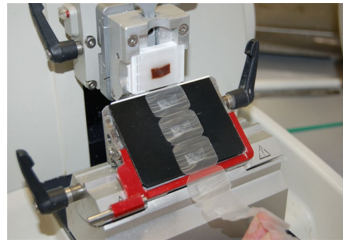
# Typical Cancer Diagnosis Process

Initial: Radiological Images

- X-Ray, CT scans, MRIs, PET

Confirmation & staging/subtyping: Pathology

- No Surgery: Needle biopsy - fine needle aspiration (FNA) or core biopsy
- Surgery and General Anesthesia: FFPE or Frozen - 1cm<sup>3</sup> cube or more tissue
  - FFPE: Formalin; Paraffin; Slicing; Staining with H&E
  - Frozen: Faster and takes few minutes - during surgery

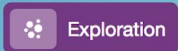


# The Data: Public TCGA (The Cancer Genome Atlas)

Harmonized Cancer Datasets

## Genomic Data Commons Data Portal

Get Started by Exploring:



Search: e.g. BRAF, Breast, TCGA-BLCA, TCGA-A5-A0G2

### Data Portal Summary

[Data Release 12.0 - August 23, 2018](#)

PROJECTS



40

PRIMARY SITES



61

CASES



32,555

FILES



356,381

GENES

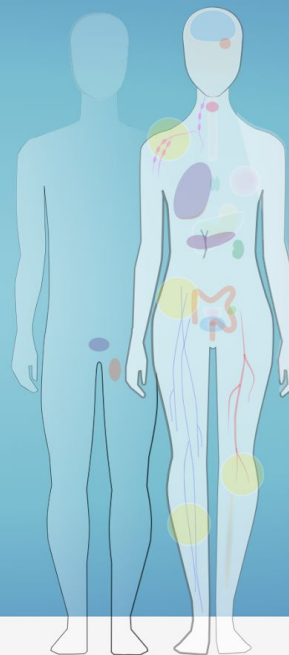


22,147

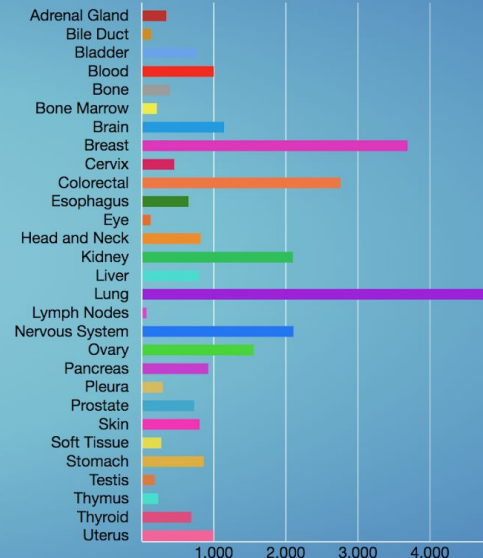
MUTATIONS



3,142,246



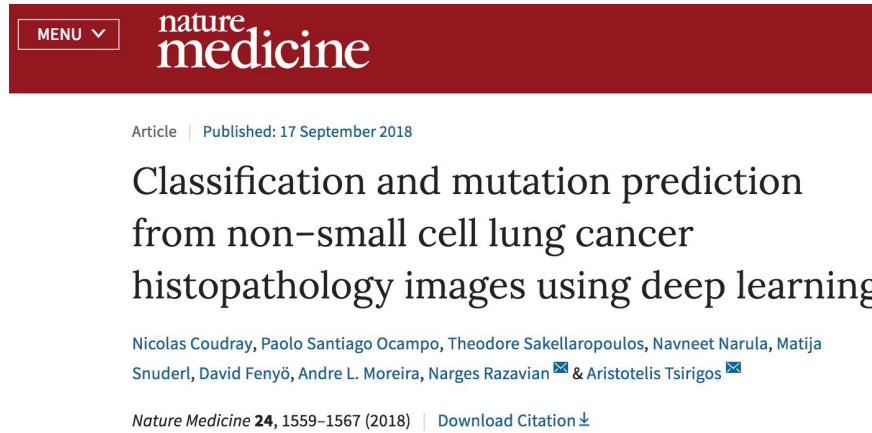
Cases by Major Primary Site



# Related work: Classification of Histopathology Images

“Classification and mutation prediction from non–small cell lung cancer histopathology images using deep learning”

<https://www.nature.com/articles/s41591-018-0177-5>

A screenshot of a Nature Medicine article page. The top navigation bar is dark red with the 'nature medicine' logo in white. Below the logo is a 'MENU' button with a downward arrow. The article title is 'Classification and mutation prediction from non–small cell lung cancer histopathology images using deep learning'. The authors listed are Nicolas Coudray, Paolo Santiago Ocampo, Theodore Sakellaropoulos, Navneet Narula, Matija Snuderl, David Fenyö, Andre L. Moreira, Narges Razavian, and Aristotelis Tsirigos. The journal information is 'Nature Medicine 24, 1559–1567 (2018)' and there is a 'Download Citation' link.

MENU ▾ nature medicine

Article | Published: 17 September 2018

## Classification and mutation prediction from non–small cell lung cancer histopathology images using deep learning

Nicolas Coudray, Paolo Santiago Ocampo, Theodore Sakellaropoulos, Navneet Narula, Matija Snuderl, David Fenyö, Andre L. Moreira, Narges Razavian & Aristotelis Tsirigos

*Nature Medicine* **24**, 1559–1567 (2018) | [Download Citation](#)

## Abstract

Visual inspection of histopathology slides is one of the main methods used by pathologists to assess the stage, type and subtype of lung

# Lung Cancer: Second most common cancer, and leading cause of cancer death

**234,000** new cases in  
2018

**154,000** deaths<sup>[1]</sup>

**80%** are *Non-Small  
Cell Lung Cancer*<sup>[2]</sup>

**EGFR mutations**

**20%** in USA/Europe

**60%** in East Asia<sup>[3-4]</sup>

**Approved  
Molecularly  
Targeted  
Therapies** for  
EGFR-mutant lung  
cancers<sup>[5-6]</sup>

[1] USA 2018 Stats, The American Cancer Society, <https://www.cancer.org/cancer/non-small-cell-lung-cancer/about/key-statistics.html>

[2] The American Cancer Society, <https://www.cancer.org/cancer/non-small-cell-lung-cancer/about/what-is-non-small-cell-lung-cancer.html>

[3] Rosell, Rafael, et al. *New England Journal of Medicine* 361.10 (2009): 958-967.

[4] <https://www.mycancergenome.org/content/disease/lung-cancer/egfr/>

[5] Shi, Yuankai, et al. *Journal of thoracic oncology* 9.2 (2014): 154-162.

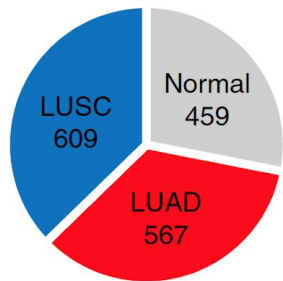
[6] <https://www.curetoday.com/articles/treatment-for-egfr-mutant-lung-cancer-is-rapidly-expanding>

# The Data

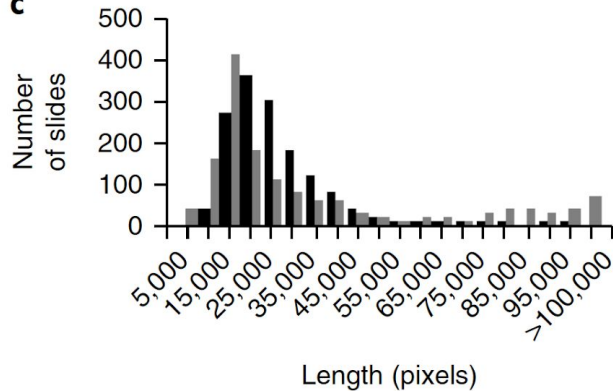
1,634 whole-slide images (1,176 tumor tissues and 459 normal tissues)

- For Adenocarcinoma, there are also mutations available

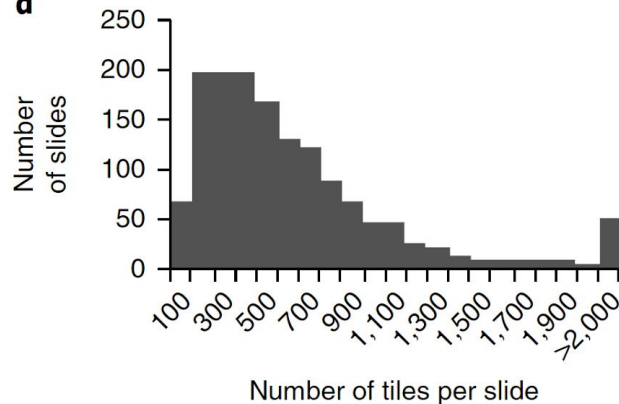
**a**



**c**



**d**





# Training, Validation, Test, Aggregation

**b**

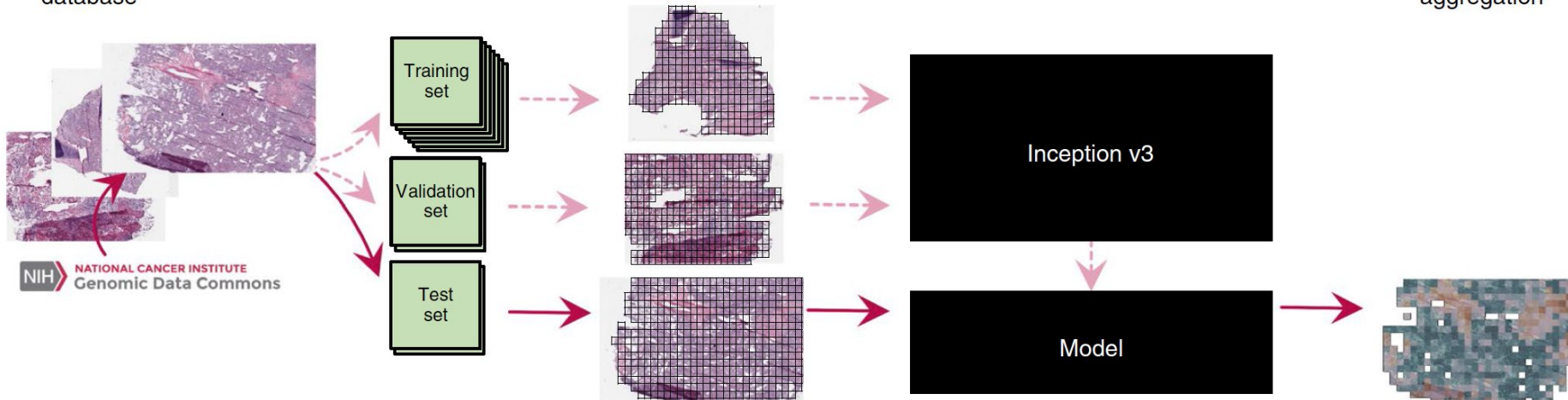
i Download from GDC database

ii Separate in 3 datasets

iii Tile and filter out background tiles

iv Per-tile training

v Testing and per-slide tile aggregation



# Results

|   |  | AUC after aggregation by...          |   |
|---|--|--------------------------------------|---|
| Classification                                  | Information  | ... average predicted probability    | ... percentage of positively classified tiles |
| <b>Normal vs Tumor (20x tiles)</b>              | a) Inception v3, fully-trained   | 0.993<br>[0.974-1.000]               | 0.990<br>[0.969-1.000]                        |
|   | b) Inception v3, transfer learning   | 0.847<br>[0.782-0.906]               | 0.844<br>[0.777-0.904]                        |
| <b>LUAD vs LUSC (20x tiles)</b>                 | c) Inception v3, fully-trained   | 0.950<br>[0.913-0.980]               | 0.947<br>[0.911-0.978]                        |
|   | d) Same as (c) but aggregation done solely on tiles classified as "tumor" by A | 0.952<br>[0.915-0.981]               | 0.949<br>[0.912-0.980]                        |
| <b>LUAD vs LUSC (5x tiles)</b>                  | Inception v3, fully-trained  | <b>0.942</b><br><b>[0.907-0.971]</b> | 0.906<br>[0.851-0.951]                        |
|   | Normal   | 0.984<br>[0.947-1.000]               | 0.985<br>[0.953-1.000]                        |
| <b>3 classes. Normal vs LUAD vs LUSC at 20x</b> | LUAD   | <b>0.969</b><br><b>[0.933-0.994]</b> | 0.970<br>[0.937-0.993]                        |
|   | LUSC   | 0.966<br>[0.935-0.990]               | 0.964<br>[0.932-0.989]                        |
|   | Micro-average  | 0.970<br>[0.950-0.986]               | 0.969<br>[0.949-0.985]                        |
|   | Macro-average  | 0.976<br>[0.949-0.993]               | 0.976<br>[0.950-0.993]                        |
| <b>3 classes. Normal vs LUAD vs LUSC at 5x</b>  | Normal   | <b>0.997</b><br><b>[0.993-0.998]</b> | 0.988<br>[0.962-1.000]                        |
|   | LUAD   | 0.965<br>[0.942-0.983]               | 0.938<br>[0.896-0.971]                        |
|   | LUSC   | <b>0.977</b><br><b>[0.960-0.991]</b> | 0.964<br>[0.937-0.986]                        |
|   | Micro-average  | <b>0.980</b><br><b>[0.972-0.987]</b> | 0.966<br>[0.948-0.980]                        |
|   | Macro-average  | <b>0.981</b><br><b>[0.968-0.991]</b> | 0.964<br>[0.939-0.980]                        |

*n=244 slides for LUAD vs LUSC classifiers and n=170 slides for the others, all from 137 patients.*

# Predicting gene mutational status from whole-slide images

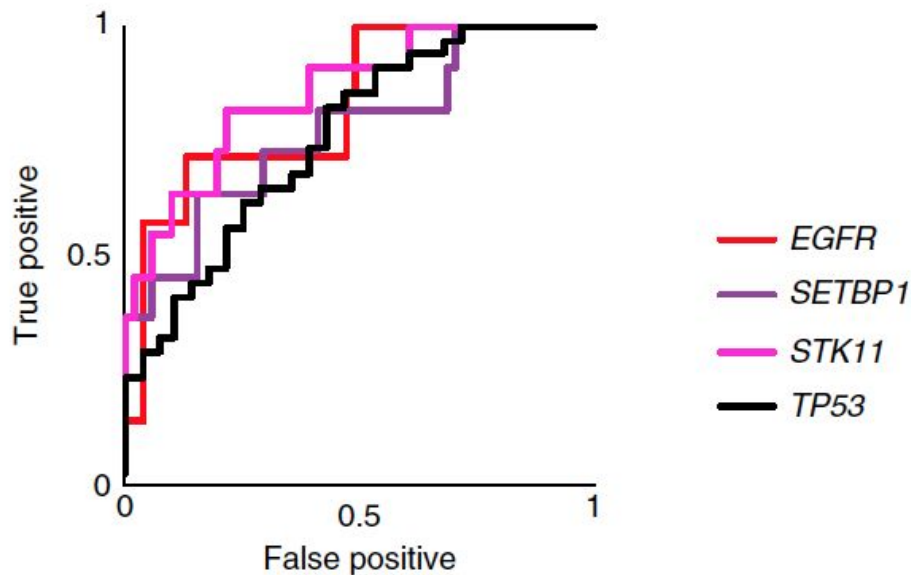


**Table 1 | AUC achieved by the network trained on mutations (with 95% CIs)**

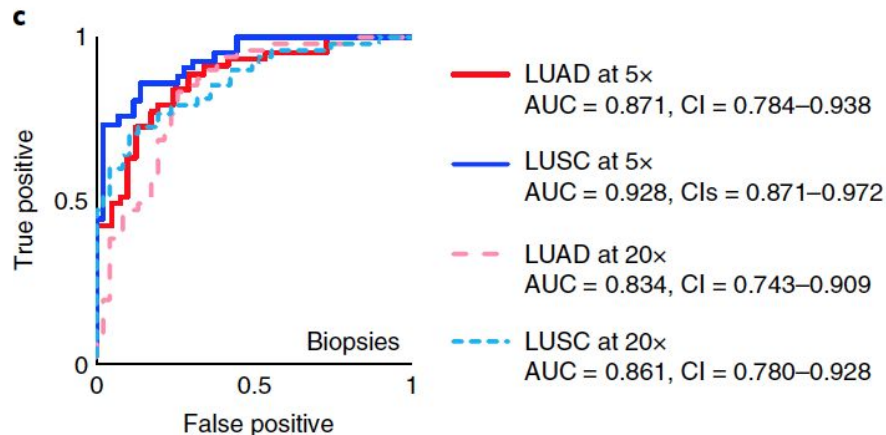
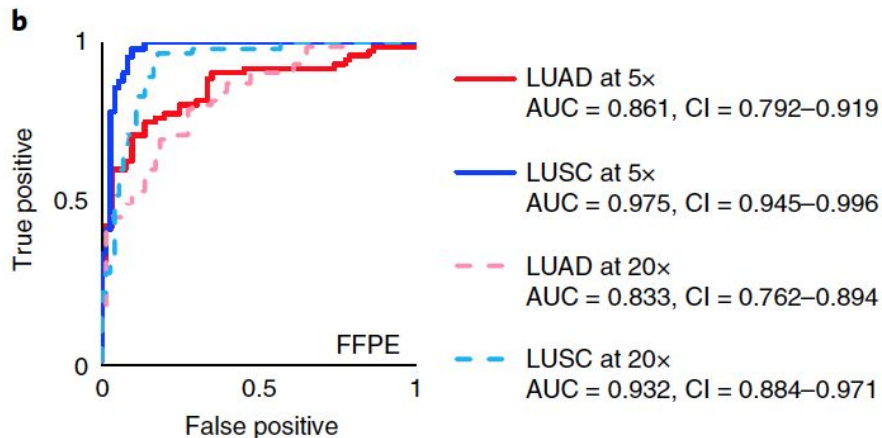
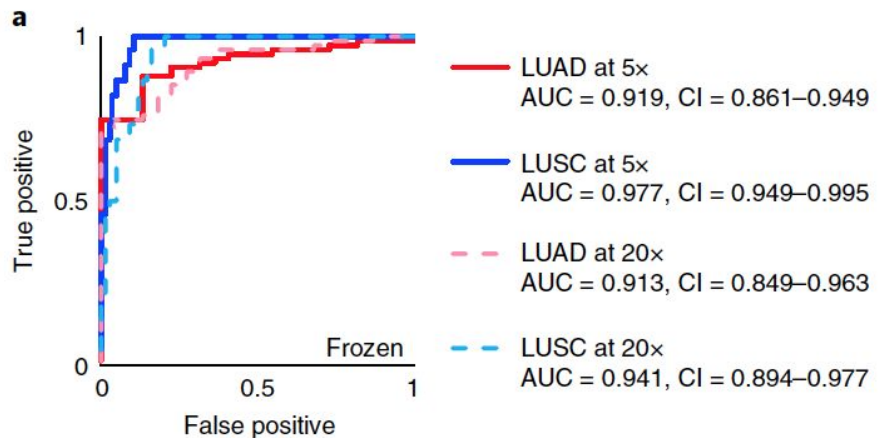
| Mutations     | Per-tile AUC        | Per-slide AUC after aggregation by... |   |
|---------------|---------------------|---------------------------------------|---|
|               |                     | ... average predicted probability     | ... percentage of positively classified tiles |
| <i>STK11</i>  | 0.845 (0.838-0.852) | 0.856 (0.709-0.964)                   | 0.842 (0.683-0.967)                           |
| <i>EGFR</i>   | 0.754 (0.746-0.761) | 0.826 (0.628-0.979)                   | 0.782 (0.516-0.979)                           |
| <i>SETBP1</i> | 0.785 (0.776-0.794) | 0.775 (0.595-0.931)                   | 0.752 (0.550-0.927)                           |
| <i>TP53</i>   | 0.674 (0.666-0.681) | 0.760 (0.626-0.872)                   | 0.754 (0.627-0.870)                           |
| <i>FAT1</i>   | 0.739 (0.732-0.746) | 0.750 (0.512-0.940)                   | 0.750 (0.491-0.946)                           |
| <i>KRAS</i>   | 0.814 (0.807-0.829) | 0.733 (0.580-0.857)                   | 0.716 (0.552-0.854)                           |
| <i>KEAP1</i>  | 0.684 (0.670-0.694) | 0.675 (0.466-0.865)                   | 0.659 (0.440-0.856)                           |
| <i>LRP1B</i>  | 0.640 (0.633-0.647) | 0.656 (0.513-0.797)                   | 0.657 (0.512-0.799)                           |
| <i>FAT4</i>   | 0.768 (0.760-0.775) | 0.642 (0.470-0.799)                   | 0.640 (0.440-0.856)                           |
| <i>NF1</i>    | 0.714 (0.704-0.723) | 0.640 (0.419-0.845)                   | 0.632 (0.405-0.845)                           |

*n* = 62 slides from 59 patients.

# Generalization to Other Cohorts

## NYULMC DATA

- Frozen sections (98 slides)
- FFPE sections (140 slides)
- Needle biopsies (102 slides)



# Comparison to Pathologists

**Supplementary Table 3. Inter-pathologists and binary deep-learning method variability estimated with the Cohen's Kappa statistic.**

|   | <i>Pathologist 1*</i>   | <i>Pathologist 2**</i>  | <i>Pathologist 3*</i>   | <i>Consensus between pathologists</i> | <i>Deep-learning</i>    |
|---|-------------------------|-------------------------|-------------------------|---------------------------------------|-------------------------|
| <i>TCGA</i>                             | 0.67<br>CIs=[0.56-8.78] | 0.70<br>CIs=[0.60-0.81] | 0.70<br>CIs=[0.59-0.81] | 0.78<br>CIs=[0.69-0.88]               | 0.82<br>CIs=[0.74-0.91] |
| <i>Pathologist 1</i>                    |                         | 0.52<br>CIs=[0.39-0.65] | 0.55<br>CIs=[0.42-0.67] | 0.56<br>CIs=[0.44-0.69]               | 0.64<br>CIs=[0.52-0.75] |
| <i>Pathologist 2</i>                    |                         |                         | 0.78<br>CIs=[0.69-0.88] | 0.65<br>CIs=[0.54-0.77]               | 0.63<br>CIs=[0.52-0.75] |
| <i>Pathologist 3</i>                    |                         |                         |                         | 0.75<br>CIs=[0.65-0.86]               | 0.60<br>CIs=[0.48-0.72] |
| <i>Consensus between 3 pathologists</i> |                         |                         |                         |                                       | 0.77<br>CIs=[0.68-0.87] |

*n=170 slides from 137 patients*

*\* thoracic pathologists; \*\* anatomic pathologist*

# Microscopy and Super-resolutions

# Cellular Imaging - Latest Updates

Recent advances in *fluorescence microscopy*:

- Tagging 100s of RNAs (corresponding to genes), Proteins, etc. in live cells
- “Seeing” across time and space at much higher resolution
- Limits on amount of light that can be given to each batch
- Light is proportional to Resolution (Similar to X-Ray radiation dose)

Will change the way we understand drug response

Will change the way we understand cellular behaviour

Applications for All Cancers, Alzheimer’s disease, Neurological conditions, etc.

# Content-Aware Image Restoration: Pushing the Limits of Fluorescence Microscopy

<https://www.biorxiv.org/content/early/2018/07/03/236463>

New Results

## Content-Aware Image Restoration: Pushing the Limits of Fluorescence Microscopy

 Martin Weigert,  Uwe Schmidt,  Tobias Boothe,  Andreas Müller,  Alexandr Dibrov,  Akanksha Jain,  Benjamin Wilhelm,  Deborah Schmidt,  Coleman Broaddus,  Siân Culley,  Maurício Rocha-Martins,  Fabián Segovia-Miranda,  Caren Norden,  Ricardo Henriques,  Marino Zerial,  Michele Solimena,  Jochen Rink,  Pavel Tomancak,  Loïc Royer,  Florian Jug,  Eugene W. Myers

doi: <https://doi.org/10.1101/236463>

This article is a preprint and has not been peer-reviewed [what does this mean?].

Abstract

Info/History

Metrics

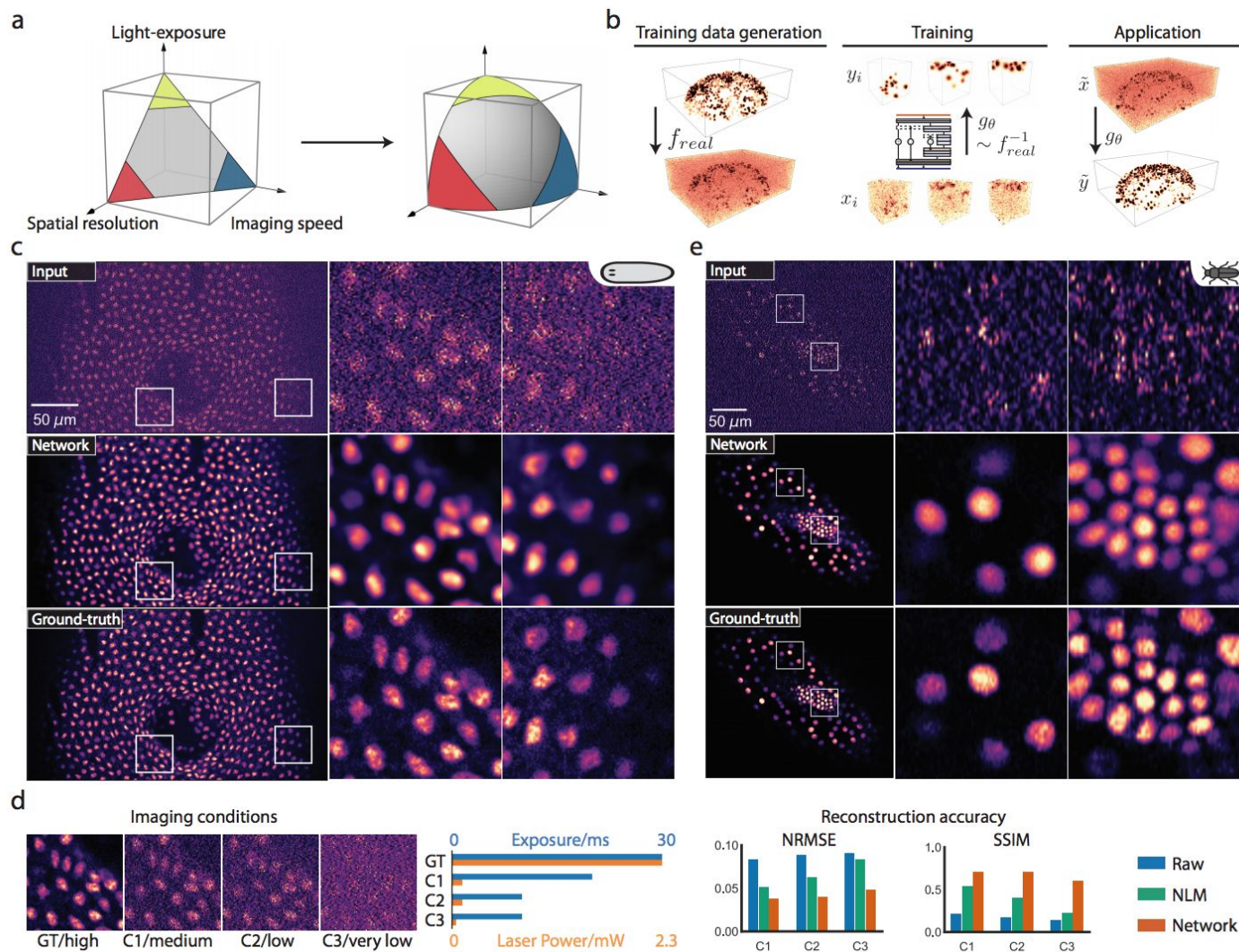
Supplementary material

 Preview PDF

### Abstract

Fluorescence microscopy is a key driver of discoveries in the life-sciences, with observable phenomena being limited by the optics of the microscope, the chemistry of the fluorophores, and the maximum photon exposure tolerated by the sample. These limits necessitate trade-offs between imaging speed, spatial resolution, light exposure, and imaging depth. In this work we show how image restoration based on deep learning extends the range of biological phenomena observable by microscopy.





# Models for Sequences and Genomics

# Biomarkers from Sequential Convolutional Nets

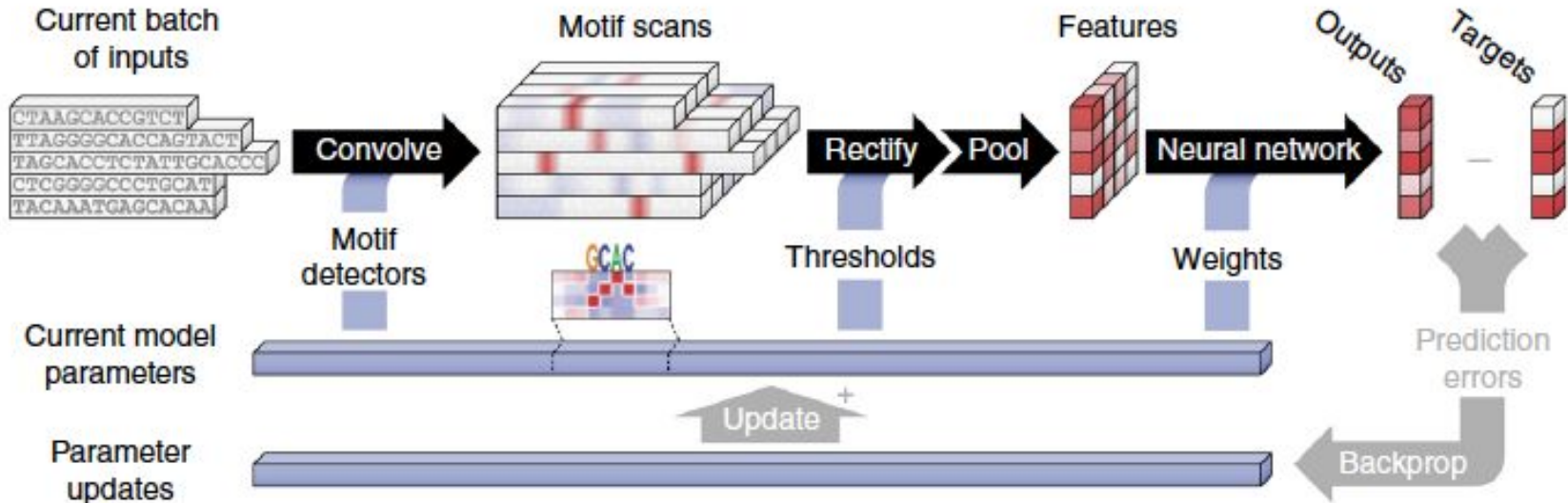
Babak Alipanahi, Andrew Delong, Matthew T Weirauch & Brendan J Frey,  
*"Predicting the sequence specificities of DNA-and RNA-binding proteins by deep learning."* Nature biotechnology (2015)

Collaboration: UToronto

Objective: Discover DNA/RNA motifs that bind to many binding proteins, and predict protein-binding in multiple tasks (in vitro and in vivo)

Data: 240,000 RNA sequences and 207 binding proteins; 40,000 DNA sequences and 86 binding proteins (transcription factors)

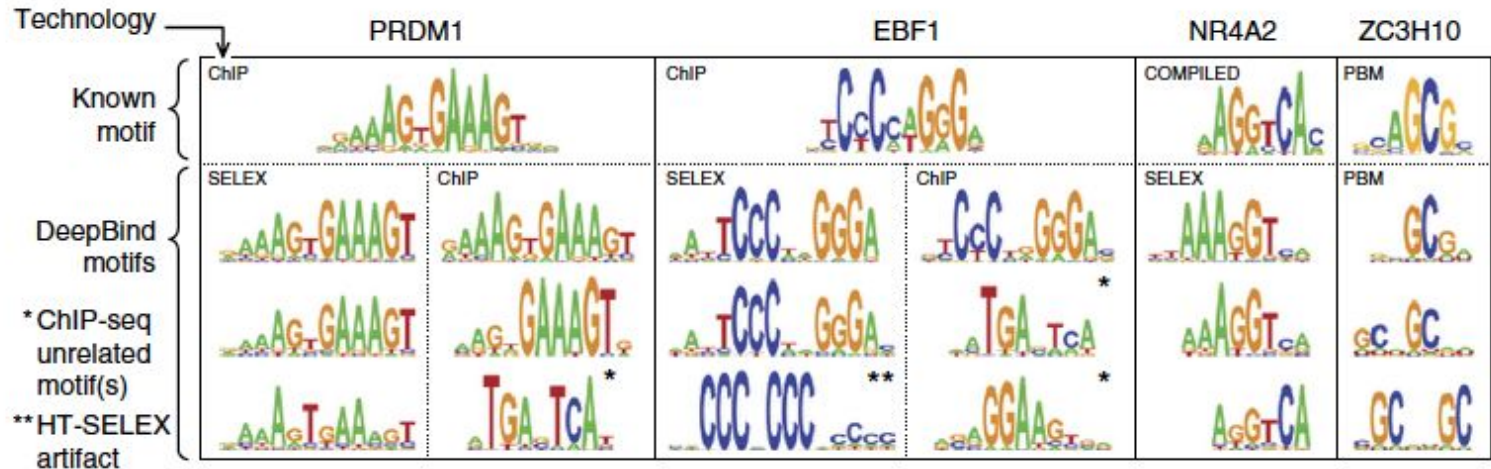
# Convolution Model for discovering Motifs and Position Weight Matrices



# Results

In vitro:

- DNA Specificity prediction; Average AUC 0.726
- RNA Specificity prediction: Average AUC 0.84



# State of Research In ML for Healthcare

## Short term and Long term

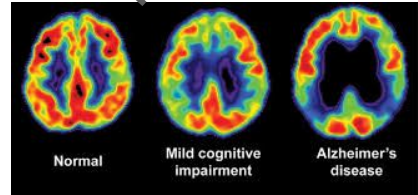
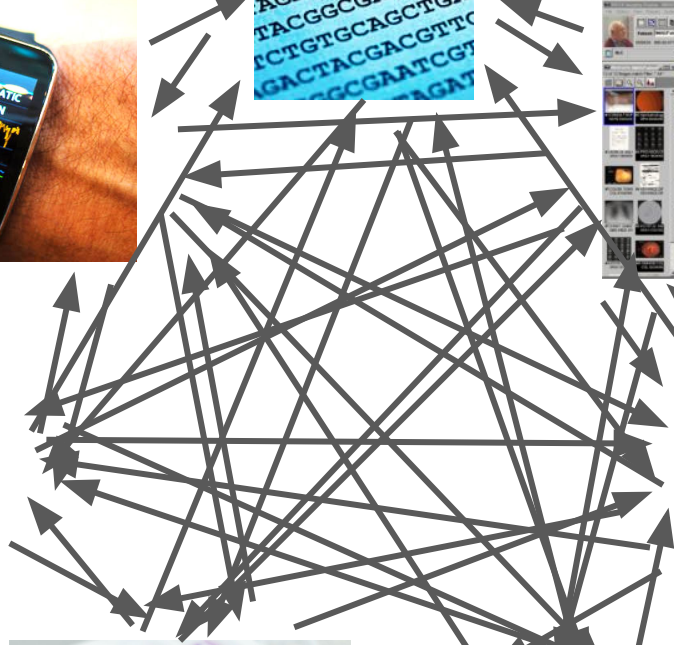
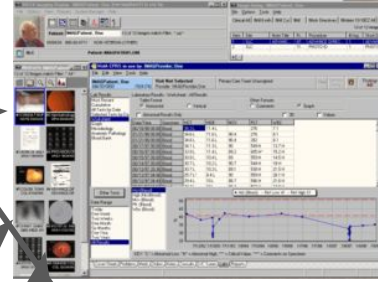
# Short term: many many standard supervised learning

It's natural & necessary to build several new baselines

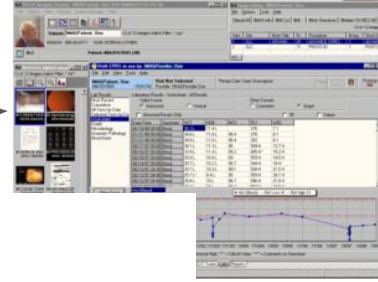
- Healthcare has recently joined data-heavy fields.
- Most baselines in other fields haven't even been tried here.
- We do need to build many many baselines.
- New architectures/models aren't necessarily needed
- Need to understand what tasks are *actually* harder and need more ML innovations

Outcome of this stage:

- Models that can be deployed in practice: shift focus to integration & system changes & industry change
- Identification of medical tasks that are actually difficult!

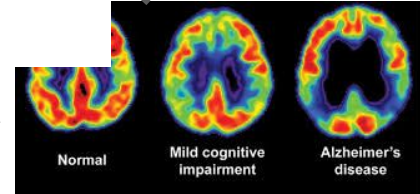






Each of these arrows learned

- Will save lives
- Will discover new hypothesis
- Will save money
- Will change industries



# What is difficult today?

Tracking and representing and modeling *changes* over time

- Predicting it, predicting with it, disentangling factors, etc.
- Even ML tools aren't mature in this area.

Recommending treatments:

- Counterfactual inference & personalized medicine

Rare diseases..

Beyond current tools:

- New sensors & hardwares - Physics & Chemistry!
- Repurposing existing hardware (i.e. MRI pulse sequences, Ultrasounds, etc)
- Embedded sensors

# That's it for now!

Email me with follow ups and questions:

**[Narges.Razavian@nyumc.org](mailto:Narges.Razavian@nyumc.org)**

Also, take the next semester's class:

**Deep Learning for Medicine**

**BMSC-GA 4493 or BMIN-GA 3007**